

# The Different Sizes of Small-Scale Robotics: from Nano- to Millimeter-Sized Robotic Systems and Applications

---

*Organizers: I. Paprotny and S. Bergbreiter*

<http://www.eecs.berkeley.edu/~igorpara/microICRA2013/>

## Objectives

There is little doubt that robotic systems that operate at nano-, micro- and millimeter scales will enable tremendous advances in areas such as medicine, information security, and microassembly. The last ten years have presented significant advances in the development of small-scale robotic systems. Surmounting inherent limitations imposed by scaling laws in small robotic systems require creative solutions that challenge the definition of robotics. How these robots operate changes dramatically as their scale changes from milli-, micro-, and finally nano-meters, e.g., the mode of operation of a centimeter sized artificial insect is diametrically different from nano-scale chemical drug-delivery.

The goal of this workshop is a forum that will bring together researchers in the field of small-scale robotics, ranging from the nano- to millimeter scales, and provide a venue to present the latest findings relating to specific applications at the different scales these robots operate. The workshop consist of talks from invited speakers representing the various size domains of small-scale robotics, followed by a moderated panel discussion. The aim is to stimulate a conversation regarding the limitations, differences and the applicant areas specific to each size regime these robots operate at, and postulate about the development in this field over the next 25 years.

## Topics of interest

- small-scale flying robots (milli, - micro)
- small-scale mobile robots (milli, micro)
- mobile microrobots
- microassembly (milli-, micro, and nano)
- biomimetic robots (milli-, micro, and nano)
- nanorobotic systems

## **Invited Speakers:**

- Zhi Ern Teoh, Harvard University, Cambridge, MA, USA.
- Kathrin E. Peyer, Institute of Robotics and Intelligent Systems, ETH Zurich, Zurich, Switzerland.
- Tian Qiu, Max Planck Institute for Intelligent Systems, Stuttgart, Germany.
- Chris Brown, University of Maryland, College Park, MD, USA.
- Christopher G. Levey, Dartmouth College, Hanover, NH, USA.
- Kyle Gilpin, Massachusetts Institute of Technology, Cambridge, MA, USA.
- Eric Diller, Carnegie Mellon University, Pittsburgh, PA, USA.
- Samuel Sanchez Ordonez, Institute for Integrative Nanosciences, IFW Dresden, Germany.
- Michael T. Tolley, Massachusetts Institute of Technology, Cambridge, MA, USA.
- Dirk Steuerwald, Laboratory of Applied Mechanobiology, ETH Zurich, Zurich, Switzerland.

## **Program**

Time	Talk
14:00 - 14:10	Introduction (workshop begins)
14:10 - 14:30	Pop-up book MEMS assembly of complex microrobots
14:30 - 14:50	Bacteria-inspired Magnetic Swimming Microrobots
14:50 - 15:10	Bioinspired wireless microrobots in fluids
15:10 - 15:30	Progress toward mobility in microfabricated microrobots
15:30 - 16:00	Coffee Break
16:00 - 16:20	Microrobot Species: a Surface MEMS Perspective
16:20 - 16:40	Robot Pebbles: Hardware and Algorithms for Millimeter-sized Autonomous Modular Robots
16:40 - 17:00	Addressing of Micro-Robot Teams and Non-Contact Micro-Manipulation
17:00 - 17:20	Tubular Nanojet engines: Smart design for smart nanorobots
17:20 - 17:35	Approaches to origami-inspired self-folding of printable robots
17:35 - 17:50	Molecular shuttles
17:50 - 18:10	Panel discussion
18:10 - 18:20	Concluding remarks (workshop adjourns)

## **Organizers**

Dr. Igor Paprotny

Berkeley Sensor & Actuator Center (BSAC)

Center for Information Technology Research in the Interest of Society (CITRIS)

Department of Electrical Engineering and Computer Sciences (EECS)

University of California

Berkeley, CA 94720

email: igorpapa@eecs.berkeley.edu

phone: +1 (802) 683 9081

Prof. Sarah Bergbreiter

Department of Mechanical Engineering (ME)

2181 Glenn L. Martin Hall

University of Maryland

College Park, MD 20910

email: sarahb@umd.edu

phone: +1 (301) 405 6506

## **Contact**

Dr. Igor Paprotny

Berkeley Sensor & Actuator Center (BSAC)

Center for Information Technology Research in the Interest of Society (CITRIS)

Department of Electrical Engineering and Computer Sciences (EECS)

University of California

Berkeley, CA 94720

email: igorpapa@eecs.berkeley.edu

phone: +1 (802) 683 9081

# Pop-up book MEMS assembly of complex microrobots

Z. E. Teoh, S.B. Fuller, A.T. Baisch and R. J. Wood

**Abstract**—Manual assembly of microrobots under a microscope often yields mechanisms with misaligned parts. This is a challenge for flapping-wing flying robots because small perturbations give rise to large applied torques. For example, 90° course changes in fruit flies executed in 100 ms, involve changes in stroke amplitude and Angle-of-Attack (AoA) on the order of 5°[1]. Yields from manual assembly are often low with significant variance among the resulting microrobots. Recent work on pop-up book MEMS has automated the folding assembly of the first generation RoboBee, raising the yield of functional microrobots by relying on the kinematics of the pop-up mechanism to eliminate misalignment of parts. Here we present the principles gleaned from pop-up assembly to fabricate second and third generations of the RoboBee. Whereas yield and variance were problems stemming from manual assembly, generation of complex tool-paths for the creation of the pop-up RoboBee, development of consistent design rules, and a lack of development software are the next challenges.

## I. DISCUSSION

The key idea of pop-up assembly is to use a single linear degree of freedom to cause a structure to transform from its two dimensional state into a three dimensional state. The robot is manufactured into a laminate that consist of two parts, the assembly scaffold and the robot itself.

There are two key mechanisms of the assembly scaffold of the pop-up RoboBee termed MoBee [2]: 1. Sarrus linkage. 2. Parallelogram linkage. The Sarrus linkage constrains two planes to remain parallel to each other as they move up or down relative to each other. This single degree of freedom drives nine internal linkages which form three four-bar parallelogram linkages. Two sets fold the wings and side frame of MoBee while the last set lifts the power actuator into place (Fig. 1). Once MoBee is assembled, it is dip-soldered causing brass pads at various fold junctions to lock. The pop-up laminate is repositioned in a laser machine that frees MoBee from the assembly scaffold.

The second generation RoboBee has two control actuators and a power actuator [3]. Manual assembly was slow, unreliable and produced RoboBees that had significant variance in their performance. In trying to apply Pop-up assembly to improve its manufacturability, a hybrid approach was taken to reduce the complexity of the laminate design. Instead of

This work was partially supported by the National Science Foundation (award numbers CCF-0926148 and CMMI-0746638) and the Wyss Institute for Biologically Inspired Engineering. Any opinions, findings, and conclusions or recommendations expressed in this material are those of the authors and do not necessarily reflect the views of the National Science Foundation.

The authors are with the School of Engineering and Applied Sciences, Harvard University, Cambridge MA 02138 USA and the Wyss Institute for Biologically Inspired Engineering, Harvard University, Boston, MA 02115, USA(E-mail: zhiernteh@seas.harvard.edu and rjwood@eecs.harvard.edu)

using a sarrus linkage driven lifting plane and three sets of parallelogram linkages, only one set of parallelogram linkages was used to lift the power actuator into the manually folded side frames which had integrated drop in control actuators (Fig. 2). The folding of the side frame and wings mimics the assembly kinematics of MoBee which will enable the automated assembly of this concept with the addition of the missing sarrus and parallelogram linkages.

As more complex mechanisms are integrated into the RoboBee, it is unclear how pop-up assembly can be used given the weight constraints imposed by the goal of creating a flight weight robot. A variation of the separate control and power actuator RoboBee uses a control actuator and a power actuator to control the (AoA) of its wings [4]. The current design uses four planar four bar linkages, two spherical four bar linkages and two spherical five bar linkages. The assembly of these linkages is done with a combination of folding stops built into the laminate and clips which enable the assembler to glue the joints with relative ease. Its assembly is manual but relies on the bulk scaffold as an assembly aid (Fig. 3), a theme that runs through all the fabrication methods presented so far.

As microrobots become more complex, the number of layers in a laminate can increase. For example, the RoboBee in Fig. 3 consist of 37 layers. Due to the complexity of the intra and inter layer relationships, a set of design rules and a series of systematic design checks have to be formulated to enable the designer to generate complex cut paths. To this end, we have come up with a rudimentary set of design checks that enable us to generate cut paths for each layer in the laminate:

- 1) Using a CAD program, create the microrobot and its associated assembly scaffold in its folded state.
- 2) Unfold the entire assembly into a 2D laminate.
- 3) For each layer in the laminate create the outline of the corresponding layer in the microrobot/assembly scaffold.
- 4) Then combine all the outlines to create a picture of all possible intersections. This picture tells us what cuts we have to make before lamination (this cuts cannot be made otherwise because it is blocked by layers on top of it.)
- 5) Go through each layer and compare the outline in each layer to the picture of intersections. Any overlap indicates that a cut has to be made.

By no means is this the best way to generate the cut files for each layer but represents a systematic way for the designer using the lamination process to built microrobots.

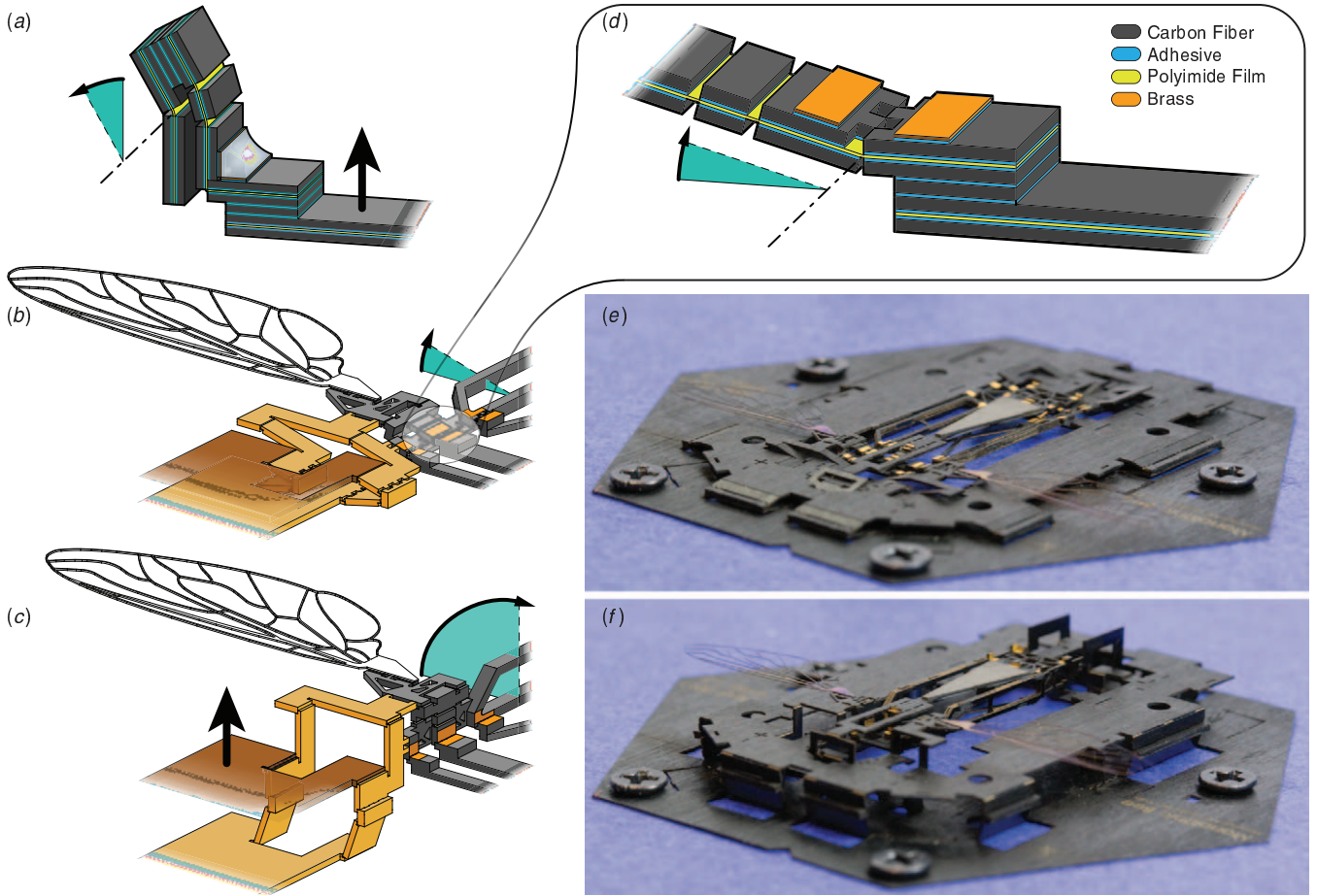


Fig. 1. Topology and folding assembly of PC-MEMS devices. (a) A four-bar linkage containing three active joints used as a transmission, turning linear actuation into rotational wing motion. (b) Schematic representation of Mobee prior to and (c) after folding assembly, illustrating how the assembly scaffold (gold) drives assembly folds with a single degree of freedom. (d) Castellated folding joints enable precision folding. (e) Mobee prior to and (f) after folding assembly. (Figure and caption taken from [2])

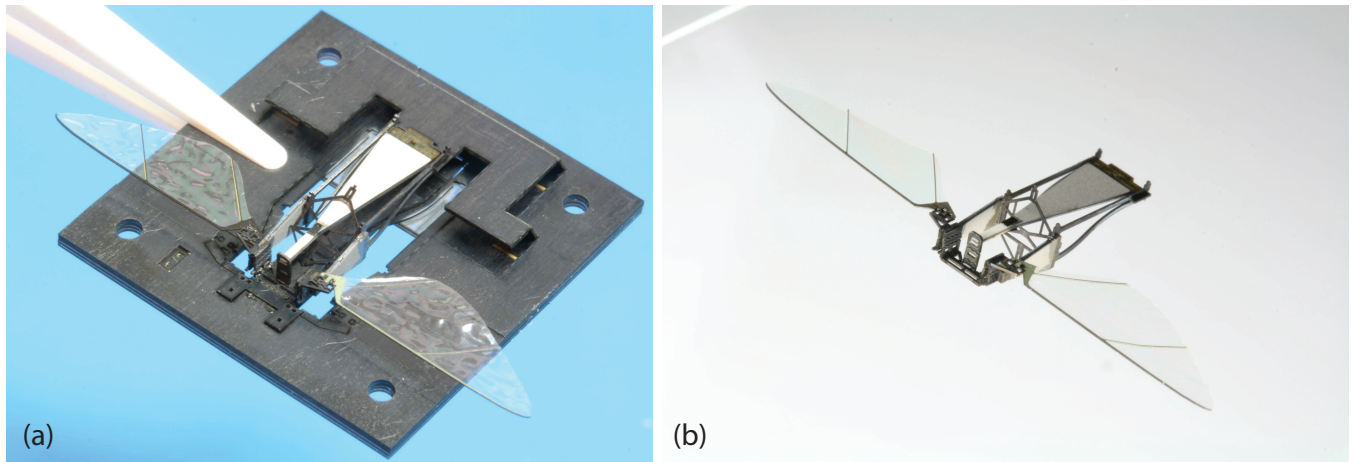


Fig. 2. RoboBee with two control actuators and one power actuator. (a) Assembly scaffold with drop in control and power actuators. (b) After release cuts.

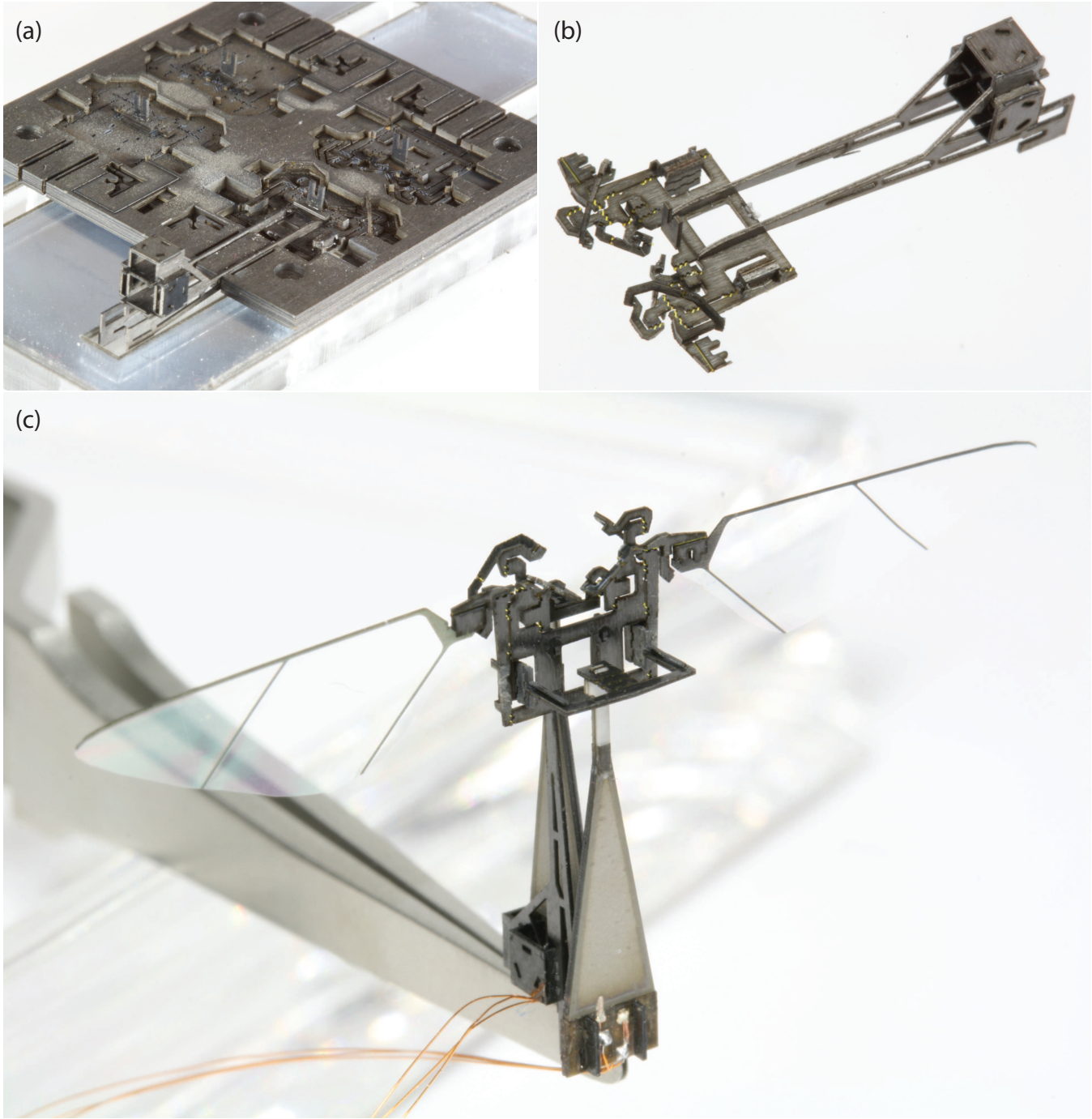


Fig. 3. RoboBee with one control and one power control. (a) Multilayered laminate containing four RoboBee thoraxes. Bottom corner of laminate shows a RoboBee spine mating with a thorax. (b) After release cuts. (c) Assembly of actuators positioned using slots and spring clips. Wings positioned with mating features at the wing hinge.

## REFERENCES

- [1] S. N. Fry, R. Sayaman, and M. H. Dickinson, “The aerodynamics of free-flight maneuvers in drosophila,” *Science*, vol. 300, no. 5618, pp. 495–498, 2003.
- [2] P. Sreetharan, J. Whitney, and R. Strauss M, and Wood, “Monolithic fabrication of millimeter-scale machines,” *Journal of Micromechanics and Microengineering*, 2012.
- [3] B. Finio and R. Wood, “Open-loop roll, pitch and yaw torques for a robotic bee,” in *Intelligent Robots and Systems (IROS), 2012 IEEE/RSJ International Conference on*. IEEE, 2012.
- [4] Z. Teoh and R. Wood, “A flapping-wing microrobot with a differential angle-of-attack mechanism,” in *Robotics and Automation (ICRA), 2013 IEEE/RSJ International Conference on*. IEEE, 2013.

# Bacteria-inspired Magnetic Swimming Microrobots

Kathrin E. Peyer<sup>1</sup>, Famin Qiu<sup>1</sup>, Soichiro Tottori<sup>1</sup>, Li Zhang<sup>2</sup>, and Bradley J. Nelson<sup>1</sup>

**Abstract**—Microrobots have recently been promoted for future minimally invasive medical procedures and as tools for studying biology at the micro-scale. The remote guidance and actuation of microrobotic devices in fluid environments by means of magnetic fields is one of the most promising approaches for *in vivo* applications. Helical microrobots mimic the propulsion method of *E. coli* bacteria, which use the rotation of helical flagella for motion generation. These swimming microrobots are actuated by a rotating magnetic field, which generates a torque around the helical axis. Methods that have been successfully employed for fabricating helical microstructures are presented and the potential of magnetic helical microrobots in biomedicine are discussed.

Swimming microrobots have the potential to be used as minimally invasive tools in medical applications, such as during eye surgery or for targeted drug delivery [1]. There are a number of challenges when designing microrobots, such as finding suitable locomotion methods and means of power supply. One of most promising actuation methods is the use of external magnetic fields. There are magnetic force-driven and torque-driven microrobot designs [2]. Helical microrobots mimic the propulsion method of *E. coli* bacteria. It is the helical shape of the flagellum that transforms the rotation into a translational motion. The bacteria use an on-board rotary motor to drive the helical flagella. Helical microrobots, commonly referred to as artificial bacterial flagella (ABFs), rely on externally applied rotating magnetic fields to generate a torque along the helical axis. They do not require additional magnetic forces.

The first magnetic helical microrobot, albeit with an overall size of several millimeters, was published in 1996 [3]. Several publications of large-scale helical microrobots followed, and it was only in 2007 that the first micro-sized helical robot was presented [4], [5]. The fabrication was based on the previously established self-scrolling technique, which allowed the controlled deformation of bi- and tri-layers of material due to internal material stresses. The first ABF design used a square nickel “head” where the magnetic torque could be applied. The choice of material for this fabrication method is, however, limited. In 2012 a very versatile fabrication method was employed by Tottori *et al.* to make micro-helices [6]. With a 3D laser writing tool arbitrary microstructures can be patterned from a variety of photosensitive polymers. The magnetic material necessary

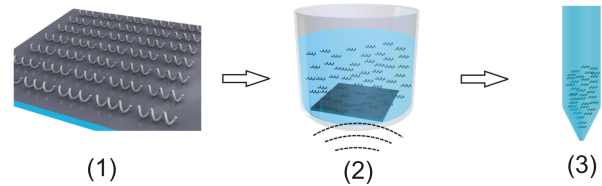


Fig. 1. Fabrication of ABF suspensions. (1) Arrays of ABFs fabricated by direct laser writing. (2) Batch release of ABFs by means of sonication. (3) Final ABF suspension. Reused with permission [4].

for the actuation was subsequently evaporated on the whole structure.

One of the main challenges for the successful application of microrobots in biomedicine is their surface functionalization. Depending on the type of application, the material should have, for example, biocompatible or anti-fouling properties. Tottori *et al.* covered the robots with a layer of titanium, which has well-known biocompatible properties, and incubation tests showed that the arrays of microrobots are non-toxic to mouse myoblast cells [6]. Biofluids contain many fibers, proteins and cells that can impede the motion of the microrobot, for example by physically obstructing the path or by adhering themselves to the surface [7]. The latter may be prevented by applying anti-fouling properties to the robot’s surface. Qiu *et al.* successfully fabricated ABF suspensions, which will allow for easy subsequent surface functionalization steps [8].

## REFERENCES

- [1] B. J. Nelson, I. K. Kaliakatsos, J. J. Abbott, Microrobots for Minimally Invasive Medicine, *Ann. Rev. Biomed. Eng.*, vol. 12, p. 55–85, 2010
- [2] K. E. Peyer, L. Zhang, B. J. Nelson, Bio-inspired Magnetic Swimming Microrobots for Biomedical Applications, *Nanoscale*, 5, pp. 1259–1272, 2013
- [3] T. Honda, K. I. Arai, K. Ishiyama, Micro Swimming Mechanisms Propelled by External Magnetic Fields, *IEEE Trans. Magn.*, 32, pp. 5085–5087, 1996
- [4] K. E. Peyer, S. Tottori, F. Qiu, L. Zhang, B. J. Nelson, Magnetic Helical Micromachines, *Chem. Eur. J.*, 19, pp. 28–38, 2013
- [5] D. J. Bell, S. Leutenegger, K. M. Hammer, L. X. Dong, B. J. Nelson, Flagella-like Propulsion for Microrobots Using a Magnetic Nanocoil and Rotating Electromagnetic Field, *Proc. IEEE Int. Conf. Rob. Autom.*, pp. 1128–1133, 2007
- [6] S. Tottori, L. Zhang, F. Qiu, K. Krawczyk, A. Franco-Obregón, B. J. Nelson, Magnetic Helical Micromachines: Fabrication, Controlled Swimming, and Cargo Transport, *Adv. Mater.*, vol. 24, no. 6, p. 811–816, 2012
- [7] K. E. Peyer, F. Qiu, L. Zhang, B. J. Nelson, Movement of Artificial Bacterial Flagella in Heterogeneous Viscous Environments at the Microscale, *IEEE Int. Conf. Intel. Robot. and System*, pp. 2553–2558, 2012
- [8] F. Qiu, L. Zhang, S. Tottori, K. Marquardt, K. Krawczyk, A. Franco-Obregón, B. J. Nelson, Bio-inspired microrobots, *Mater. Today*, 465, 2012

<sup>1</sup> Institute of Robotics and Intelligent Systems, ETH Zurich, 8092 Zurich, Switzerland {peyer,k, qiu,f, tottoris, bnelson} at ethz.ch.

<sup>2</sup> The Chinese University of Hong Kong, Shatin NT, Hong Kong SAR (China) lizhang at mae.cuhk.edu.hk.

# Bioinspired wireless microrobots in fluids

Tian Qiu, Udit Choudhury, Hyeon-Ho Jeong, Debora Schamel, and Peer Fischer, *Member, IEEE*

**Abstract**— Building, powering, and operating structures that can navigate complex fluidic environments at the sub-mm scale is challenging. We discuss some of the limitations encountered when translating actuation mechanisms and design-concepts from the macro- to the micro-scale. Here we present a system of polymeric micro-screws that can be produced by micro-injection molding and that can be wirelessly driven by an external rotating magnetic field through biological phantoms, such as agarose gels with speeds of  $\sim 200 \mu\text{m/s}$ . The molding technique faithfully reproduces features down to a few microns. The micro-screw can serve as a model system to study minimally invasive surgical procedures, and serves as an efficient propeller for self-powered wireless microrobots in complex fluids. The fabrication scheme may readily be extended to include medically approved polymers and polymeric drug carriers.

## I. INTRODUCTION

Moving through fluid environments at the scale of micro-organisms presents a different set of challenges compared to those encountered by macroscopic swimmers. Particularly, at low Reynolds number ( $\text{Re} \ll 1$ ), which indicates a Stokes regime of fluid flow with a dominance of viscous forces over inertial forces, it is known that a simple reciprocating time reversible motion will not result in any net displacement of the swimmer [1]. Hence, asymmetric non-reciprocating actuation mechanisms are required at low  $\text{Re}$ . Micro-organisms use two non-reciprocal propulsion mechanisms: the travelling wave beats of cilia and the helical rotation of flagella.

Mimicking a rotating flagellum requires a rotary motor and power source capable of producing sufficient torque to overcome the high viscous drag at low Reynolds number. One may consider the use of electromagnetic motors, which are ubiquitous in macro-scale robotics. However, electromagnetic motors require sizeable currents which preclude miniaturization. One of the smallest commercial electromagnetic motors is thus still 6 mm long with a diameter of 1.9 mm [2]. This is too large for applications in micro-surgery. Piezoelectric rotary motors do not require large currents and piezoelectric elements can readily be obtained that have small linear dimensions ( $\sim 250 \mu\text{m}$ ), but they require relatively high input voltages  $\sim 28 \text{ V}_{\text{pp}}$  [3]. If the motor is to be powered wirelessly using a battery, then this presents a problem, as thin film lithium ion batteries typically supply microampere currents at 1-3 V which corresponds to  $\mu\text{W}$  (for an area of  $\sim 20 \text{ mm}^2$ ). Similarly, microfuel cells would require at least  $1 \text{ cm}^2$  to produce power in the range of

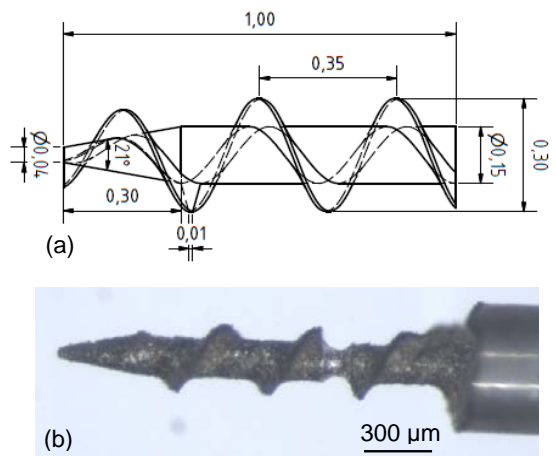
mW [4]. There are therefore no simple compatible combinations of motor and onboard powering source for designing sub-mm micro-swimmers. Hence, we resort to external magnetic fields and the torque they exert on structures that contain a permanent magnet. Published methods used in the fabrication of magnetically-actuated helical micro-propellers are:

- i)  $1 - 2 \mu\text{m}$ : Glancing angle deposition with electron beam evaporation [5]
- ii)  $10 \mu\text{m}$ : Direct laser writing of helical structures [6]
- iii)  $40 \mu\text{m}$ : Metallic thin film strain engineering techniques [7]

Although all of these techniques can manufacture precise helical flagella or screw-like structures, they are primarily wafer-based processes which require relatively complex setups. In order to produce low-cost helical screws at sub-mm scale, we present a bench-top micro-molding scheme that is able to produce polymeric micro-screws. The choice of materials can thus be extended to medically approved polymers.

## II. EXPERIMENTAL RESULTS

The metal micro-screw is prepared by electrical discharge machining (EDM). As shown in Fig. 1, the micro-screw is designed to have an outer diameter of  $300 \mu\text{m}$  in order to fit inside a 23 gauge needle (nominal inner diameter  $337 \mu\text{m}$ ). Hardened steel is used as the template. The EDM process is time-consuming and is limited to conducting materials, which may not be suitable for medical applications. We have therefore developed a micro-molding process that uses a single EDM machined template from which polymer micro-screws may be batch-produced.



\*Research supported by the Max Planck Society and the European Research Council under the ERC Grant agreement 278213.

T. Qiu, U. Choudhury, H. Jeong, D. Schamel, and P. Fischer are with the Max Planck Institute for Intelligent Systems, 70569 Stuttgart, Germany (corresponding author P. Fischer, phone: 0711-689-3560; fax: 0711-689-3412; e-mail: fischer@is.mpg.de).

Figure 1. The metal template for micro-molding process. (a) Schematic drawing of micro-screw design. Sizes are in mm. (b) Scanning electron

microscope image of the micro-screw template manufactured by electro-discharge machining (EDM).

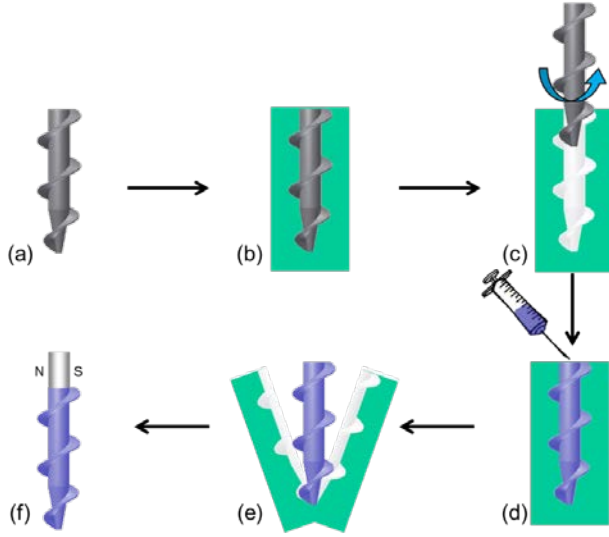


Figure 2. Illustration of the micro-molding process. (a) Metal template by EDM. (b) Micro-molding using PVS. (c) After curing of the PVS mold, removal of the metal template. (d) Polymer injection and curing. (e) Unmolding by splitting the PVS mold. (f) Magnet attachment.

The micro-molding process consists of 6 steps, as illustrated in Fig. 2. First, the metal template is manufactured by an EDM process (collaboration with the Institut für Mikrotechnik in Mainz, Germany) (Fig. 2(a)). Then Polyvinyl siloxane (PVS) impression material (Art. No 4667, Coltene Whaledent, Switzerland) is mixed and the metal template is inserted (Fig. 2(b)). After 5 min curing, the metal template is removed (Fig. 2(c)). Cycloaliphatic Epoxide Resin (ERL-4221 Modified SPURR Embedding Kit, SERVA Electrophoresis GmbH, Heidelberg, Germany) is then injected into the mold (Fig. 2(d)). After the epoxy is cured at 70°C for 3 hours, the PVS mold is cut and split, and the polymer micro-screw is released (Fig. 2(e)). Finally, a cylindrical NdFeB micro-magnet (200 µm in diameter and 400 µm in length) is attached to the end of the polymer (Fig. 2(f)). By this cheap and fast micro-molding process, the micro-structure of the metal template is precisely replicated.

To test the magnetic micro-screw, we have used a tri-axial Helmholtz coil that can generate fields of up to 80 Gauss at up to 100 Hz (Fig. 3). We use custom LabView software to control the amplitude and direction of the rotating magnetic field in 3D. To mimic the rheological properties of biological tissue we prepare various agarose gels for *in vitro* testing. Fig. 4 shows a micro-screw that is propelled in a 0.1%wt agarose gel. The trajectory is defined in real time by a joystick (see Fig. 4(d)). The average linear velocity reaches roughly 200 µm/s with a magnetic field rotating at 5 Hz.



Figure 3. Helmholtz coil setup to drive the micro-screw. (a) Tri-axial Helmholtz coil setup is used to drive and steer the micro-screw. Stereo-microscope (Leica MZ95 stereomicroscope with a Leica DFC 490 camera) is used to observe the movement. (b) 3-dimensional navigation of the micro-screw can be realized by turning the magnetic field with a joystick. (c) Enlarged picture of the tri-axial Helmholtz coil.

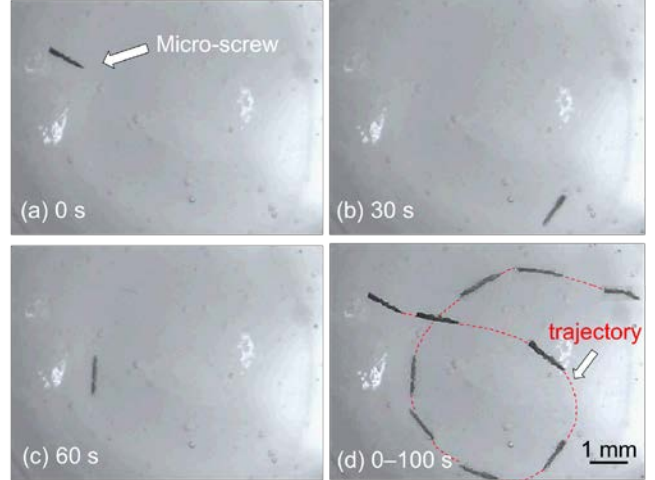


Figure 4. Propulsion of the micro-screw in agarose gel (0.1% wt) at 5 Hz. Snapshots after (a) 0 s, (b) 30 s, (c) 60 s, respectively, (d) the trajectory of the micro-screw from 0 to 100 s defined by the external magnetic field.

### III. CONCLUSION

We have demonstrated controlled propulsion of a polymer micro-screw in agarose gels. The fabrication is convenient and scalable and permits larger numbers of screws to be obtained quickly. The micro-molding process can serve as a cost-effective replication method for microrobot propellers.

The micro-screws have the potential to be used as an efficient propeller for self-powered wireless microrobots in fluids. The system may serve as a promising micro-tool for minimally invasive surgery, and the fabrication scheme is general such that it permits the use of medically approved

Polymer materials. The latter can further be loaded with suitable molecules and drugs.

#### ACKNOWLEDGMENT

The authors thank C. Miksch for helpful suggestions and for assistance with the micro-molding setup, and B. Miksch for assistance with the joystick control algorithms.

#### REFERENCES

- [1] E. M. Purcell, "Life at Low Reynolds-Number," *American Journal of Physics*, vol. 45, pp. 3-11, 1977.
- [2] [http://www.micromo.com/datasheets/BrushlessDCmotors/0206\\_B\\_DF\\_F.pdf](http://www.micromo.com/datasheets/BrushlessDCmotors/0206_B_DF_F.pdf)
- [3] B. Watson, J. Friend and L. Yeo, "Piezoelectric ultrasonic resonant motor with stator diameter less than 250  $\mu\text{m}$ : the Proteus motor," *Journal of Micromechanics and Microengineering*, vol.19, 022001, 2009.
- [4] K. A. Cook-Chennault, N. Thambi and A. M. Sastry, "Powering MEMS portable devices - a review of non-regenerative and regenerative power supply systems with special emphasis on piezoelectric energy harvesting systems," *Smart Materials and Structures*, vol. 17, 043001, 2009.
- [5] A. Ghosh and P. Fischer "Controlled Propulsion of Artificial Magnetic Nanostructured Propellers," *Nano Letters*, vol.9, no.6, pp. 2243-2245, 2009.
- [6] S. Tottori, L. Zhang, F. Qiu, K. K. Krawczyk, A. Franco-Obregón and B. J. Nelson "Magnetic Helical Micromachines: Fabrication, Controlled Swimming, and Cargo Transport," *Advanced Materials*, vol.24, no.6, pp. 811-816, 2012.
- [7] L. Zhang, J. J. Abbott, L. Dong, B. E. Kratochvil, D. Bell and B. J. Nelson (2009). "Artificial bacterial flagella: Fabrication and magnetic control," *Applied Physics Letters*, vol. 94, 064107, 2009.

# Progress toward mobility in microfabricated microrobots

Sarah Bergbreiter, Aaron P. Gerratt, and Dana Vogtmann

**Abstract**— Research on mobile microrobots has been ongoing for the last 20 years, but the few robots that have walked have done so at slow speeds on smooth silicon wafers. However, ants can move at speeds over 40 body lengths/second on surfaces from picnic tables to front lawns. What challenges do we still need to tackle for microrobots to achieve this incredible mobility? This abstract presents some of the mechanisms that have been designed and fabricated to enable robot mobility at the insect size scale. These mechanisms utilize new microfabrication processes to incorporate materials with widely varying moduli and functionality for more complexity in smaller packages. Results include a 4mm jumping mechanism that can be launched over 30 cm straight up, preliminary leg designs, and an actuated jumping mechanism used as a catapult.

## I. DISCUSSION

In biology, it is not uncommon to find impressive locomotion in small packages. Cockroaches can run at speeds up to 50 body lengths per second [1] and ants less than 5 mm long have been demonstrated running at speeds approaching 40 body lengths per second [2]. Insects like the flea and froghopper can jump to heights over 100x their own length [3]. This impressive mobility in insects is due in part to complex mechanisms packaged at very small size scales.

One way that nature generates these mechanisms is through the incorporation of various biological materials from resilin to chitin to muscle. These materials can allow for high strains and nonlinearities resulting in seemingly complex behavior. However, microrobots, defined as sub-centimeter sized robots with microscale features, are typically built using microelectromechanical systems (MEMS) and microfabrication [4], [5], [6], [7], [8], [9], [10]. Since MEMS were derived from the same techniques used to build integrated circuits, they are often limited to the same materials as integrated circuits - typically silicon, silicon dioxide, silicon nitride, polysilicon, and metals [11]. These materials are brittle, limited to strains of several percent, and have moduli of 10s to 100s of GPa. The biological material that enables jumping in many insects is resilin. This material can undergo large strains, has a modulus of approximately 2 MPa, and is highly resilient (approximately 97% of energy is returned when deformed) [12]. It is promising to consider the benefits of adding compliant materials like resilin to microrobot design.

At larger scales, bio-inspired robots have taken advantage of a wide array of materials to provide the same passive mechanical properties used by insects at smaller scales. For

example, iSprawl was manufactured using the shape deposition manufacturing process in which materials with various properties were combined to create complex mechanisms such as a passive hip joint for rapid locomotion [13]. RHeX maintained its mobility across a variety of terrains by taking advantage of the passive compliance of its legs [14]. A joint made of carbon fiber and polyimide resulted in an additional passive degree of freedom that enabled in the first liftoff of a centimeter-scale flapping robot [15].

Microrobots made from traditional MEMS materials, however, lack the robustness of their biological cousins. The microrobot in [16] often lost legs due to brittle  $2\mu\text{m}$  square polysilicon pin hinges. However, the only legged microrobot that has demonstrated forward motion also displayed impressive robustness, in part due to the use of polymer legs made from a combination of polyimide and silicon [6].

A key challenge in microrobotics is the addition of new materials to the currently existing microfabrication toolbox for manufacturing complex mechanisms and substantially improving locomotion. Poly(dimethylsiloxane) (PDMS) is a compliant material that can undergo elastic strains in excess of 100% and has a Young's modulus of 1.8 MPa [17], which is very similar to that of resilin. PDMS is most commonly used to quickly and easily fabricate small and clear channels for fluid flow in microfluidics and bioMEMS [18]. However, it has rarely been used for its mechanical properties, primarily because of the lack of adequate fabrication processes. Parylene has been used to replace silicon springs given its modulus of 1 GPa [19], but this is still a relatively stiff, non-elastic material. Polyimide has been used for its thermal properties in the microrobot legs mentioned above [6].

This work discusses the application of the first microfabrication processes to incorporate compliant elastomer structures in-plane with traditional silicon microelectromechanical systems. By incorporating new materials, elastomer springs are applied as compact energy storage mechanisms for small jumping robots. The fabrication process for an 8 mg, 4 mm x 4 mm x 0.3 mm jumping mechanism (Fig. 1) is shown in Fig. 2. The device stored  $100\mu\text{J}$ , 40% of which was transferred into kinetic energy of the mechanism resulting in jump heights as high as 32 cm (Fig. 3). A similar fabrication process (Fig. 4) was used to fabricate an actuated system on an SOI chip (Fig. 5). This thermally actuated device stored and released  $0.45\mu\text{J}$  to propel a 1.4 mg projectile more than 7 cm (Fig. 6). Preliminary leg designs are also shown in this process (Fig. 7). The jumping mechanism and the actuated mechanism were both used repeatedly to store and release energy, demonstrating the enhanced mechanical robustness of the devices manufactured with these processes.

S. Bergbreiter, A. P. Gerratt, and D. Vogtmann are with the Department of Mechanical Engineering and the Institute for Systems Research, University of Maryland, College Park, MD 20742 USA [sarahb@umd.edu](mailto:sarahb@umd.edu)

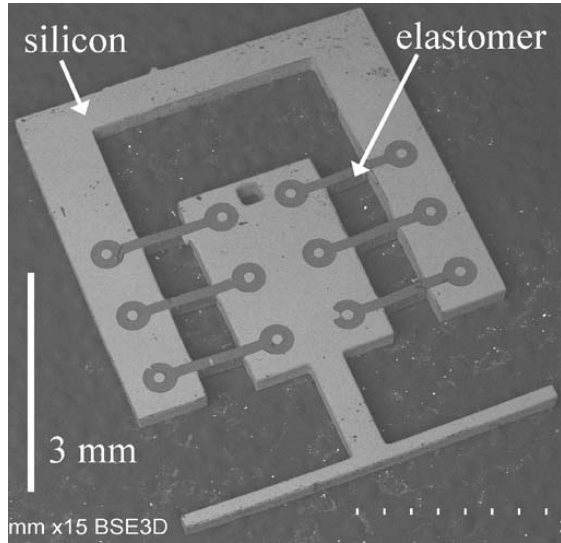


Fig. 1. SEM image of a jumping mechanism [20].

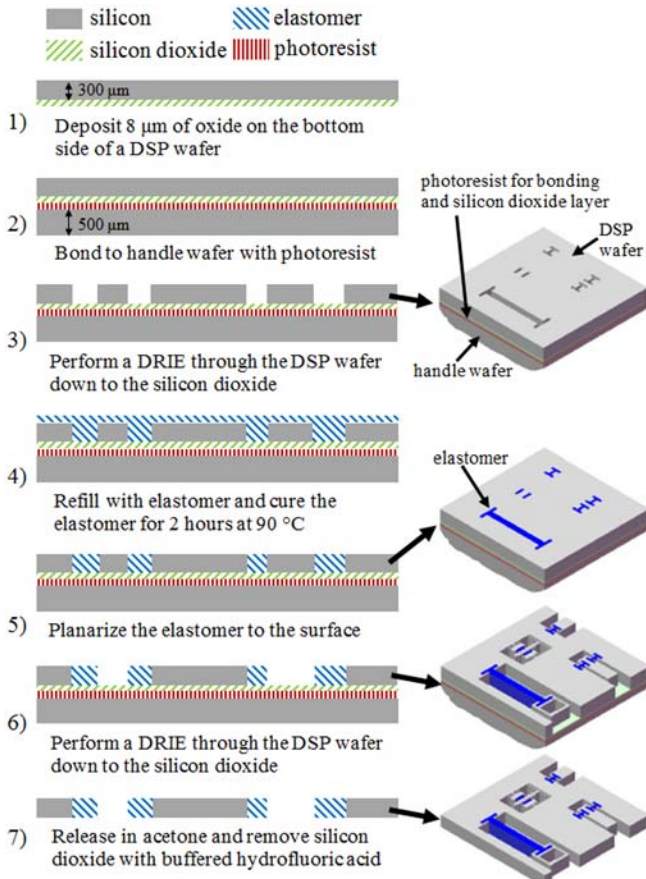


Fig. 2. Cross-section and perspective views of the DSP-based fabrication process [20].

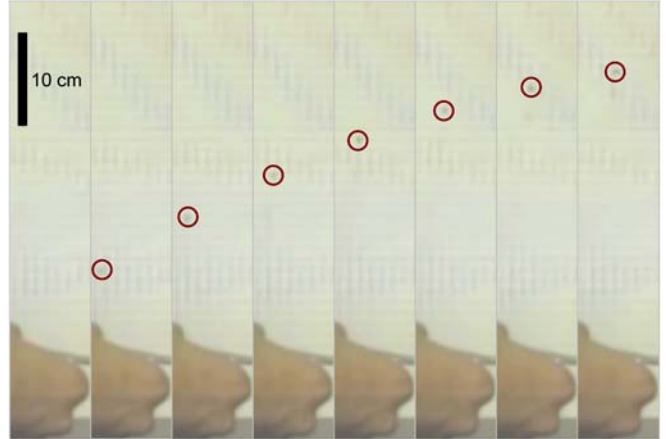


Fig. 3. Screenshots from a video showing the takeoff of the jumping mechanism. Due to the small size of the jumping mechanism relative to the scale of the jump, the mechanism is difficult to make out, but it has been circled in each frame to show the position [20].

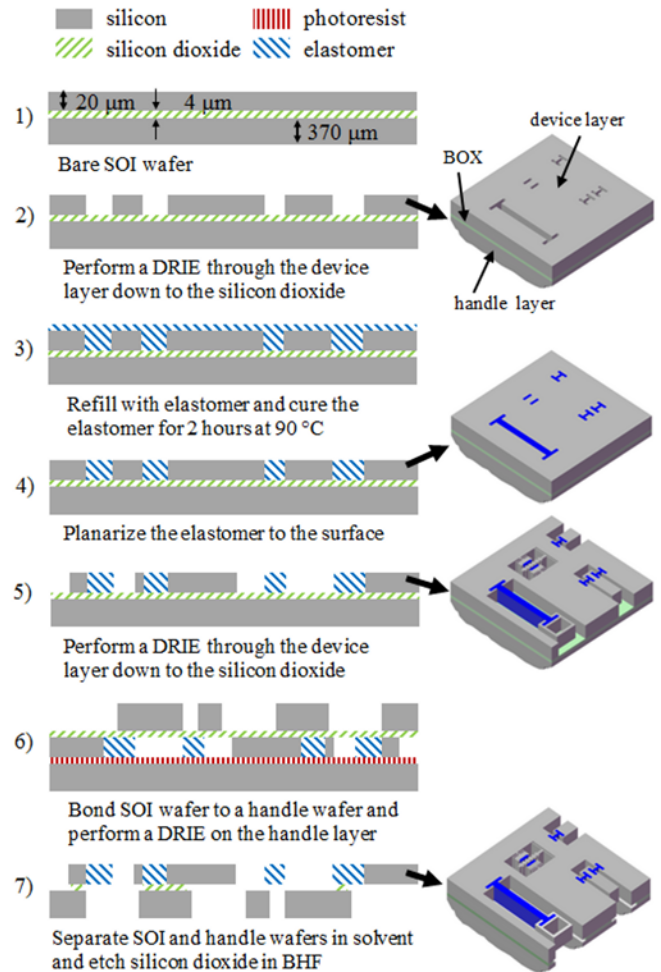


Fig. 4. Cross-section and perspective views of the SOI-based fabrication process [20].

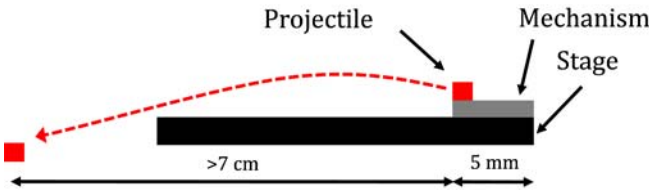


Fig. 6. A schematic of the test setup. The projectile was placed on top of the wafer substrate, which was placed on a stage under a microscope [20].

## II. ACKNOWLEDGMENTS

The authors gratefully acknowledge the support of the Maryland NanoCenter and its FabLab. This work was partially supported under DARPA YFA grant no. HR0011-08-1-0043, NSF Award #CNS0931878, and Award #ECCS1055675.

## REFERENCES

- [1] R J Full and M S Tu, "Mechanics of a rapid running insect: two-, four- and six-legged locomotion," *The Journal of Experimental Biology*, vol. 156, pp. 215–231, 1991.
- [2] T Seidl and R Wehner, "Walking on inclines: how do desert ants monitor slope and step length," *Frontiers in Zoology*, vol. 5, no. 1, pp. 8, 2008.
- [3] M Burrows, "Froghopper insects leap to new heights," *Nature*, vol. 424, pp. 509, 2003.
- [4] A P Gerratt, I Penskiy, and S Bergbreiter, "SOI/elastomer process for energy storage and rapid release," *Journal of Micromechanics and Microengineering*, vol. 20, no. 10, pp. 104011, 2010.
- [5] P Dario, R Valleggi, M C Carrozza, M C Montesi, and M Cocco, "Microactuators for microrobots: a critical survey," *Journal of Micromechanics and Microengineering*, vol. 2, no. 3, pp. 141–157, 1992.
- [6] T Ebefors, J U Mattsson, E Kalvesten, and G Stemme, "A walking silicon microrobot," in *International Conference on Solid-State Sensors, Actuators, and Microsystems (Transducers)*, Sendai, Japan, June 1999, pp. 1202–1205.
- [7] W S N Trimmer, "Microrobots and micromechanical systems," *Sensors and Actuators*, vol. 19, no. 3, pp. 267–287, 1989.
- [8] B R Donald, C G Levey, C D McGraw, I Paprotny, and D Rus, "An untethered, electrostatic, globally controllable MEMS microrobot," *Journal of Microelectromechanical Systems*, vol. 15, no. 1, pp. 1–15, 2006.
- [9] R Yeh, E J J Kruglick, and K S J Pister, "Surface-micromachined components for articulated microrobots," *Journal of Microelectromechanical Systems*, vol. 5, no. 1, pp. 10–17, 1996.
- [10] E Y Erdem, Y-M Chen, M Mohebbi, J W Suh, G T A Kovacs, R B Darling, and K F Bohringer, "Thermally actuated omnidirectional walking microrobot," *Journal of Microelectromechanical Systems*, vol. 19, no. 3, pp. 433–442, 2010.
- [11] K E Petersen, "Silicon as a mechanical material," *Proceedings of the IEEE*, vol. 70, no. 5, pp. 420–457, 1982.
- [12] H C Bennet-Clark, "Energy storage in jumping insects," in *The Insect Integument*, H R Hepburn, Ed., pp. 421–443. Elsevier Scientific Publishing Company, Amsterdam, 1976.
- [13] S Kim, "iSprawl: design and tuning for high-speed autonomous open-loop running," *The International Journal of Robotics Research*, vol. 25, no. 9, pp. 903–912, 2006.
- [14] U Saranli, M Buehler, and D E Koditschek, "RHex: a simple and highly mobile hexapod robot," *International Journal of Robotics Research*, vol. 20, no. 7, pp. 616–631, 2001.
- [15] R J Wood, "The first takeoff of a biologically inspired at-scale robotic insect," *IEEE Transactions on Robotics*, vol. 24, no. 2, pp. 341–347, 2008.
- [16] S Hollar, S Bergbreiter, and K S J Pister, "Bidirectional inchworm motors and two-DOF robot leg operation," in *International Conference on Solid-State Sensors, Actuators, and Microsystems (Transducers)*, Boston, MA, USA, June 2003, pp. 262–267.
- [17] F Schneider, T Fellner, J Wilde, and U Wallrabe, "Mechanical properties of silicones for MEMS," *Journal of Micromechanics and Microengineering*, vol. 18, no. 6, pp. 065008, 2008.
- [18] Y Xia and G M Whitesides, "Soft lithography," *Annual Review of Materials Science*, vol. 28, no. 1, pp. 153–184, 1998.
- [19] Y Suzuki and Y. C. Tai, "Micromachined high-aspect-ratio polyimide spring and its application to low-frequency accelerometers," *Journal of Microelectromechanical Systems*, vol. 15, no. 5, pp. 1364–1370, 2006.
- [20] Aaron P Gerratt and Sarah Bergbreiter, "Incorporating compliant elastomers for jumping locomotion in microrobots," *Smart Materials and Structures*, vol. 22, no. 1, pp. 014010, Jan. 2013.

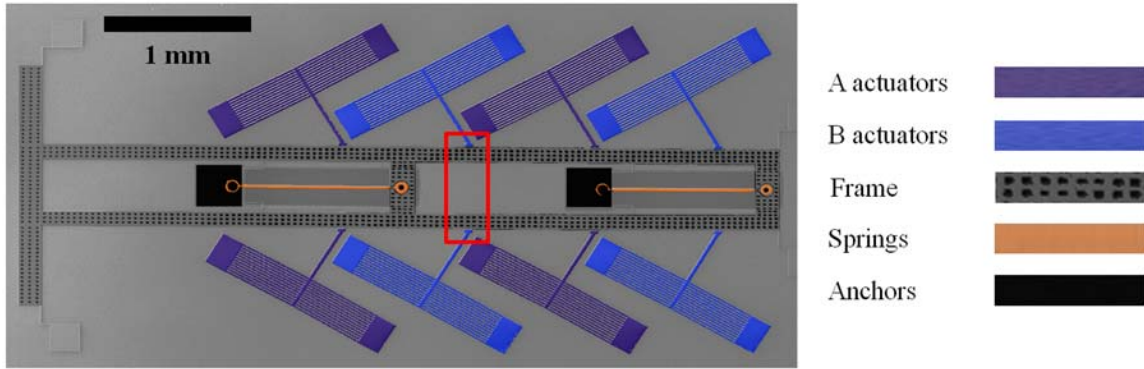


Fig. 5. A colored SEM image of the actuated mechanism. The blue and purple areas are the two sets of actuators. The orange areas are the springs. The black areas are the anchors for the springs. The patterned gray area is the frame.

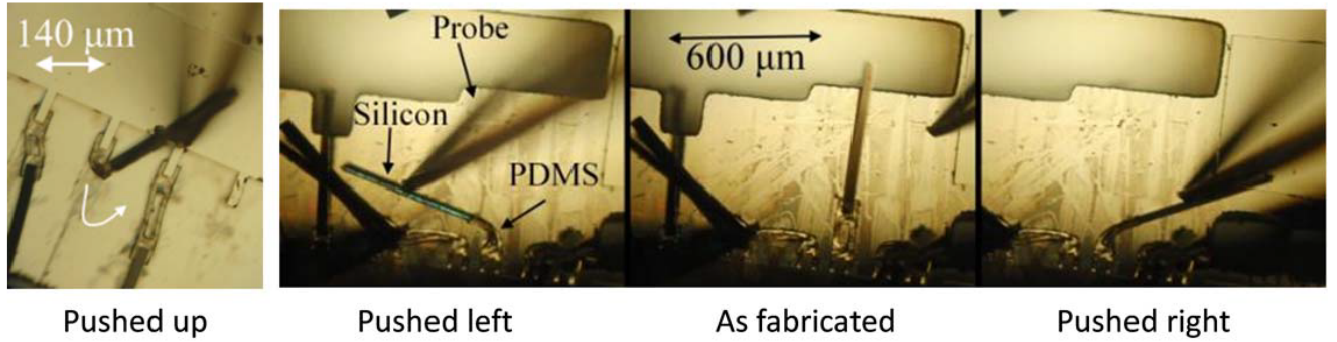


Fig. 7. Preliminary leg hinges in SOI-based fabrication process.

# MicroStressBot Species: a Surface MEMS Perspective

C. G. Levey, I. Paprotny, and B. R. Donald

**Abstract**— In this paper we review our ongoing research on untethered stress-engineered microrobots (MicroStressBots), focusing on the challenges and opportunities of operating mobile robots on the micrometer size scale. The MicroStressBots with planar dimensions of approximately 260  $\mu\text{m} \times 60 \mu\text{m}$  and a total mass less than 50 ng are fabricated from 2-4  $\mu\text{m}$  thick polycrystalline silicon using a surface micromachining processes. A single global power delivery and control signal is broadcast to all our robots, but decoded differently by each species using onboard electromechanical memory and logic. We review our design objectives in creating robots on the microscale, and describe the constraints imposed by fabrication, assembly, and operation of such small robotic systems. Our robots have been used to motivate and demonstrate multiple robot control algorithms constrained by a single global signal with a limited number of distinct voltages.

## I. INTRODUCTION

Microscale mobile devices have many potential applications, including assembly, medicine, and surveillance. The ability to operate multiple microrobots is particularly useful, but challenging to implement using a globally broadcasted control signal. In this paper we review our ongoing research effort on untethered stress-engineered microrobots (MicroStressBots) [1-5], and discuss the challenges and opportunities of operating mobile microrobots at the micrometer size scale. Specifically, we show the application of our robots to controllable microassembly tasks, and discuss the challenges and opportunities of operating robots at the microscale.

Our work is motivated by a goal to develop self-reconfigurable robotic systems at the microscale. This research objective required the development of untethered micro-scale robots with a means of (1) planar locomotion and steering, (2) wireless reception of control and power signals, and (3) on-board control signal decoding (requiring minimal memory), all operating in an environment where multiple robots could interact. To obtain this functionality in

Research supported in part by the NIH (grant numbers GM-65982, GM-78031, and NS-79929), the Office for Domestic Preparedness, Department of Homeland Security, USA (grant number 2000-DT-CX-K001), the Center for Information Technology Science in the Interest of Society (CITRIS), and the Thayer School of Engineering.

C. G. Levey (corresponding author) is with the Thayer School of Engineering at Dartmouth College, Hanover, NH, 03755, USA (phone: 603-646-2071, email: c.levey@dartmouth.edu).

I. Paprotny is with the Center for Information Technology Science in the Interest of Society and the Berkeley Sensor & Actuator Center, University of California Berkeley, CA, USA.

B. R. Donald is with the Department of Computer Science, Duke University, USA; and the Department of Biochemistry and the Duke Institute for Brain Sciences, Duke University Medical Center, USA.

a robust mass manufacturing process on the micro-scale, design simplicity is key; here the limitations of a simple elegant hardware design are compensated for by more complex control algorithms [4,5].

## II. MICROSTRESSBOTS

The MicroStressBots consist of a single monolithic plate of polycrystalline silicon with a thin chromium film used to control its out-of-plane shape through stress engineering. Precise design of each microrobot chassis and stress engineering layer ensures the ability to control multiple robots on a single substrate. Fig. 1 shows micrographs of two types MicroStressBots, a single arm design (left) and a dual arm design (right). In both cases, locomotion is accomplished using an untethered scratch drive actuator (USDA) [1], while turning occurs through a snap-down of one of the steering arms.

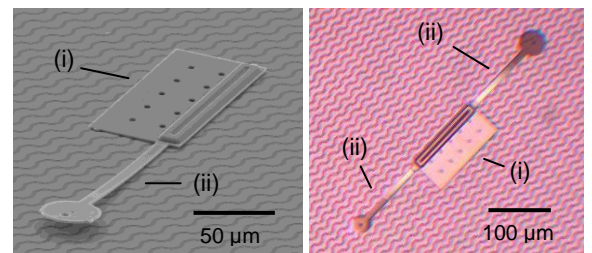


Figure 1: Micrographs of two MicroStressBots: single arm design (left) and dual-arm design (right). In both cases the untethered scratch-drive actuator (i) provides forward motion, while the steering arm actuator (ii) determines whether the robot moves forward or turns.

All the robots operate on a single power delivery substrate (also called their operating environment). Because of this, a single power and control signal is broadcast over the entire operating environment. Independent control is achieved by differentiating the design of the steering-arm actuators, and thus the behavior of the robots during the application of the global control signal. Fig. 2 shows several MicroStressBots operating on a single substrate.

### A. Locomotion

Scratch drive actuation is a well-established MEMS locomotion mechanism (see left panel, Fig. 3). Traditionally, a voltage is applied to the actuator through direct contact using a power rail or a tether wire. Our goal was to implement interacting robots without the constraints of such tethers or tracks, so we devised the capacitive coupling scheme shown in Fig. 3, right panel [1]. Broadcast electrodes are interdigitated uniformly under the entire operating environment, and are powered by a single voltage wire ( $V_2$ ) and ground ( $V_1$ ). The electrodes are covered by a

thin insulating layer (primarily zirconia). This prevents any direct electrical contact between the electrodes and the robots, and the high dielectric constant ( $\approx 20$ ) of zirconia enhances the surface charge resulting from applied voltages.

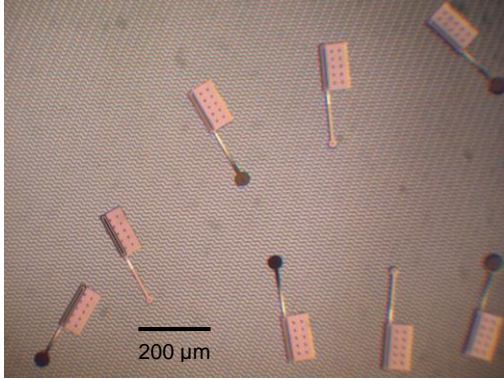


Figure 2: Multiple MicroStressBots operating on a single power-delivery substrate. The different designs of the steering-arm actuators ensure different behavior during application of a single global control signal.

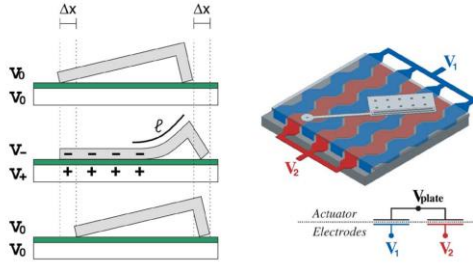


Figure 3: Untethered Scratch Drive Actuator (USDA): (left) Schematic showing one step of a scratch drive actuator, deformed by an applied voltage. (right) The power delivery substrate allows *untethered* operation through capacitive coupling [1].

A robot positioned on top of this dielectric layer covering several of the interdigitated electrodes will experience a downward force each time a voltage is applied across the electrodes. The scratch drive mechanism illustrated in left panel of Fig. 3 then converts this downward force to lateral motion [6].

### B. Steering

MicorStressBots use an electrostatic snap-down mechanism for steering as well as locomotion; both actuators are fabricated out of the same layers of doped polysilicon. The turning mechanism is shown in Fig. 4. During pull-down, a portion  $s$  of the steering arm comes into flat contact with the substrate (Fig. 4.a). When the USDA is subsequently actuated,  $s$  acts as a temporary anchor, restricting the motion of the tip of the steering arm. The robot follows a curved trajectory, flexing the steering arm until the restoring force of the arm equals the force applied by the USDA (Fig. 4.b). When the arm is released during periodic polarity reversal of the waveform, the flexure in the arm is relieved, resulting in a net change in the heading of the microrobot (Fig. 4.b). The amount of the steering arm

flexure is highly dependent on the geometry of the steering arm actuator, making the corresponding turning rate design-specific.

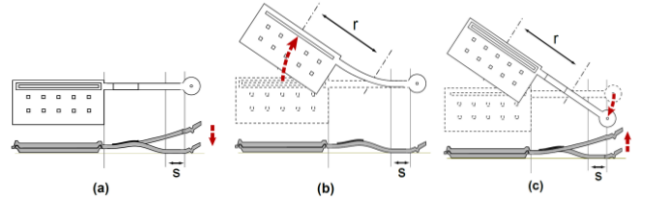


Figure 4: Turning mechanism of the MicroStressBot. (a) The steering arm is electrostatically pulled into contact with the substrate, and a flat region  $s$  is temporarily anchored in place. (b) The USDA is actuated, causing the steering arm to flex while the robot follows a trajectory with the radius of curvature  $r$ . (c) As the arm is released during a polarity reversal of the drive voltage waveform, the flexure of the steering arm is released. This cycle is continuously repeated, causing the robot to turn.

To control the actuation of the steering-arm independently of the scratch drive, we utilize electromechanical hysteresis by designing the arms to respond to different voltage levels. The scratch drive stepping voltages are nested between the steering arm snap-down voltage,  $V_d$ , and snap-up voltage,  $V_u$ , such that the scratch drive can provide locomotion with the steering arm either up or down. In [2] we show that this nesting is difficult to achieve using ordinary photolithographic patterning, which defines only the in-plane ( $x-y$ ) shape of the steering arm. However, by widening the design space to include out-of-plane ( $z$  axis) geometries, it is possible to incorporate nesting. We integrate such 3D designs into the nominally 2D process of surface micromachining by inducing out-of-plane curvature in the steering arm through stress-engineering: a stressor film is deposited on the arm and patterned in post-processing [7].

### C. Species Differentiation

While all our robots receive the same power and control signals, we can vary the design of the steering-arms of the individual MicroStressBots such that different robots respond differently to the global applied control. We call this concept for *Global Control, Selective Response* (GCSR) [3], and MicroStressBots that exhibit different behavior are said to be of a different microrobot species.

For example, the different design of the steering arms (primary varying the length of the arm, the length of the stress-engineering layer, and the pad size) result in distinct threshold voltages for changes in arm state, that is, the snap-down ( $V_d$ ) and snap-up ( $V_u$ ) voltages. Each species has a unique  $V_d$  or  $V_u$ ; control signals with different combinations of these will result in distinct motion of the individual devices. Fig. 5. shows five unique waveforms, called control primitives, which are used to differentiate the motion of four distinct microrobot species using differences in the snap-down and release voltages of their steering arms.

It is also possible to differentiate microrobot species using differences in their turning radius rather than snap voltages

[5]. Fig. 6 shows the designs (top) and trajectories (bottom) of two MicroStressBot species differentiated by their turning rates.

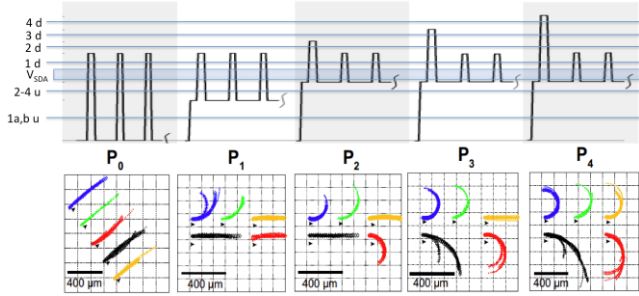


Figure 5: Differentiation of MicroStressBot species using snap-down and release voltages of the steering arms: Five unique waveform primitives,  $P_0$ - $P_4$  (top) that differentiate the motion of four different species of MicroStressBots ( $R_1$ - $R_4$ ), distinguished by their snap-down (1d-4d) and up (1u-4u) voltages. Under each control primitive are the experimental trajectories of five robot designs responding to that primitive. Clockwise from top-left of each panel except  $P_0$ , they are:  $R_{1a}$  (blue),  $R_{1b}$  (green),  $R_4$  (yellow),  $R_2$  (red),  $R_3$  (black). Robots  $R_{1a}$  and  $R_{1b}$  are different designs but belong to the same MicroStressBot species. (Based on data from [3]).

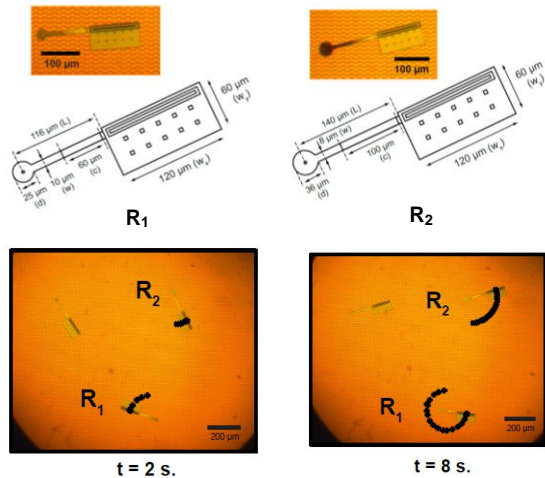


Figure 6: Differentiation of MicroStressBot species using different turning rates: The design of two different microrobot species  $R_1$  and  $R_2$  (top) and the trajectories showing their different turning rates. (bottom) (Based on data from [5])

#### D. Independent Control and Microassembly

Differentiation of microrobot species allows the MicroStressBots to be independently maneuverable within a planar operating environment. This feature has been used to implement planar microassembly, where the robots come together to form larger structures. The asymmetric friction of the USDAs (they move forward but not backwards) together with compliance allows the structures to align to a global minimum energy shape through a form of pairwise self-assembly. Fig. 7 shows five structures assembled using species differentiated by different steering arm snap voltages [3].

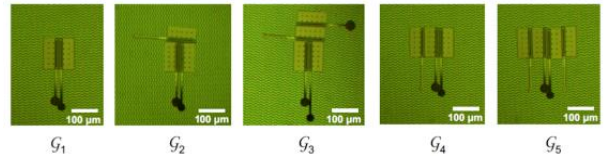


Figure 7: Five structures assembled using species differentiated by distinct snap-down and release voltages of the steering arms [3].

### III. MICROSTRESSBOT TRIBOLOGY

USDAs require non-symmetric friction in order to ensure continuous forward motion. Although they move reliably in one direction (as is clearly shown in Fig. 5), this locomotion mechanism is not yet fully understood. We have observed two surface effects that may shed light on this.

#### A. Substrate Modification

The USDAs modify the surface on which they move. Left panel of Fig 8 shows atomic force micrographs of the  $\text{SiO}_2$ -coated  $\text{ZrO}_2$  insulated surface of the power delivery substrate after traversal by a MicroStressBot. Debris pushed forward by the bushing is clearly visible. Scratches in the surface, caused either by asperities or lodged debris, can also be seen.

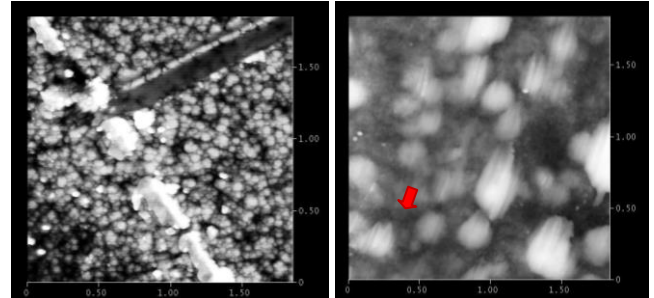


Figure 8: AFM images showing substrate modifications by scratch drive actuation: (left) Visible is the line of debris pushed by the bushing and scratches in the surface caused by either asperities in the bushing or lodged debris. (right) Apparent asperity modification for an area that has been repetitively traversed in one direction (indicated by red arrow). The grey scale corresponds to an elevation of 100 nm (black to white). The x-, and y-scale is in  $\mu\text{m}$ .

Fig. 8 (right panel) shows a close-up on the asperities on a surface that has been successively traversed by a scratch drive actuator (SDA). The asperities are elongated in the direction of travel, with a sharper edge on the side corresponding to the forward direction. Such surface modifications could contribute to the asymmetric friction observed. The statistical nature of this process is consistent with recent observations by McGraw et. al. [8] showing a distribution of USDA single step sizes.

#### B. Surface Charge Injection

The high electric field generated by the power delivery and control signal across the dielectric layer may also cause changes in the environment traversed by a MicroStressBot. Fig. 9 shows scanning electron micrographs of a tethered SDA after repetitive actuation over a silicon nitride coated surface. The SEM image reveals a shadow of the SDA,

which is likely caused by embedded charges. Charging of the substrate was also confirmed by the need for periodic polarity reversal of the power delivery waveform, although the effect was never completely negated. Such surface-embedded charges could also contribute to the asymmetry of friction of the USDA.

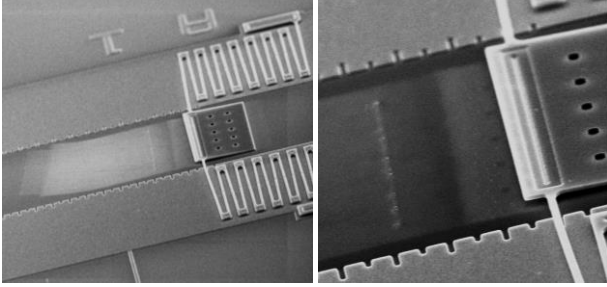


Figure 9: Scanning Electron Micrograph (SEM) images of tethered SDA after repetitive actuation over a silicon nitride surface. The shadowy image of the SDA is visible in the underlying substrate does not show up in optical microscopy, and is believed to be caused by charges embedded in the surface). Debris pushed by the bushing is also visible in both images.

#### IV. SCALING LAWS AT THE MICROSCALE

Choice mechanisms of operation and construction techniques for microrobots depend on their characteristic length scale, parametrized by  $l$  [9]. Effects which scale with volume ( $l^3$ ), such as inertia and gravitational forces play a much less important role on a microscale than they do for larger sized objects, while surface forces, friction forces, and electrostatic forces (assuming a constant electric field limited by dielectric breakdown) all scale as area ( $l^2$ ) and tend to dominate for microscale devices. The effects of any capillary forces, which scale linearly with  $l$  can be stronger yet but are difficult to utilize. We minimize the potentially deleterious effects of capillary forces by strictly operating in a dry environment. Magnetic forces from constant current density electromagnets scale with  $l^4$  and become relatively weaker on the microscale. If two permanent magnets are used, their contact force scales as ( $l^2$ ); such a system with only permanent magnets could be used for assembly but not for dynamic control. Microrobots made of hard magnetic materials can successfully interact with external field gradients[10,11]; the force then scales with magnet volume ( $l^3$ ).

A locomotion mechanism based on local electrostatic forces is thus attractive for microrobots, both because such forces are relatively large at this scale and because they scale in the same way as the dominant dissipation (friction), allowing a range of different sized robots to operate similarly within this regime. Inertial ( $\propto l^3$ ) and rotational inertia ( $\propto l^5$ ) effects are less dominant at this scale, simplifying the robot kinematics. Scratch drives provide perhaps the simplest electrostatic MEMS locomotion mechanism, but traditionally have required a tether or track to provide power. Our thin film capacitive power coupling scheme [1] enables their untethered use. This harvesting of power from the operating

environment is advantageous over schemes involving on-board energy storage because storage capacity scales with  $l^3$ , making it less usable at microscale.

Micromechanical assembly techniques are limited; our designs are fabricated as a complete unit to avoid the need for assembly. We provide locomotion, steering, power reception, and command decoding all through a simple monolithic structure. Connected transfer frames [3] enable post-fabrication placement of multiple robots as a parallel process.

#### V. CONCLUSIONS

We have fabricated a number of microrobot species using surface micromachining. Power and control signals are broadcast to the robots from a uniform global environment through capacitive coupling. MicroStressBot species are differentiated by their design, respond uniquely to the same global control signal, and are able to achieve assembly. Fabrication of mobile robots on the microscale is challenging, however the lack of mass assembly tools at this scale also provides a niche which may eventually be filled using such microrobots. On a micro-factory floor, an army of simple robots could be used to assemble more sophisticated devices out of micromachined parts.

#### REFERENCES

- [1] B. R. Donald, C. G. Levey, C. D. McGraw, D. Rus, and M. Sinclair, "Power delivery and locomotion of untethered micro-actuators," *J. Microelectromech. Syst.*, vol. 12, no. 6, pp. 947–959, Dec. 2003.
- [2] B. R. Donald, C. G. Levey, C. McGraw, I. Paprotny, and D. Rus, "An untethered, electrostatic, globally controllable MEMS micro-robot," *J. Microelectromech. Syst.*, vol. 15, no. 1, pp. 1–15, Feb. 2006.
- [3] B. R. Donald, C. G. Levey, and I. Paprotny, "Planar Microassembly by Parallel Actuation of MEMS Microrobots", *J. Microelectromechanical Syst.*, vol. 17, no. 4, pp.789-808, Aug. 2008.
- [4] B. R. Donald, C. G. Levey, I. Paprotny, and D. Rus, "Planning and control for microassembly of structures composed of stress-engineered MEMS microrobots" *The International Journal of Robotics Research*;32 pp. 218-246, Feb. 2013.
- [5] I. Paprotny, C. G. Levey, P. K. Wright, and B. R. Donald, "Turning-rate selective control: a new method for independent control of stress-engineered MEMS microrobots", *Robotics Science and Systems (RSS'12)*, Sydney, Australia, July 9-13, 2012.
- [6] T. Akiyama and K. Shono, "Controlled stepwise motion in polysilicon microstructures," *J. Microelectromech. Syst.*, vol. 2, pp. 106–110, Sep. 1993.
- [7] C.-L. Tsai and A. K. Henning, "Out-of-plane microstructures using stress engineering of thin films," *Proc. Microlithogr. Metrol. Micromach.*, vol. 2639, pp. 124–132, 1995.
- [8] C. D. McGraw, S. M. Stavis, J. Giltinan, E. Eastman, S. Firebaugh, J. Piepmeyer, J. Geist, and M. Gaitan, *J. Microelectromech. Syst.*, vol. 22, no. 1, pp. 115–123, Feb. 2013.
- [9] W. S. N. Trimmer, "Microrobots and micromechanical systems", *Sensors and Actuators*, vol. 19, no. 3, pp. 267-287 (Sept. 1989).
- [10] C. Pawashe, S. Floyd, and M. Sitti, "Multiple Magnetic Microrobot Control using Electrostatic Clamping," *Applied Physics Letters*, vol. 94, p. 161408, 2009
- [11] K. B. Yesin, K. Vollmers, and B. J. Nelson "Modeling and control of untethered biomicrorobots in fluid environment using electromagnetic fields" *International Journal of Robotics Research*, vol. 25, no. 5, pp. 527–536, 2006.

# Robot Pebbles: Hardware and Algorithms for Millimeter-sized Autonomous Modular Robots

Kyle Gilpin and Daniela Rus

## I. INTRODUCTION

The concept of programming software has been refined, popularized, and become ubiquitous. We propose moving beyond programming software to programming the properties of physical matter. Since their advent, computers have changed from mainframes, to laptops, to smart phones. We see programmable matter as the next step in this progression. For this to become a reality, we must make additional progress towards miniaturizing existing programming matter systems. Advances in both hardware and algorithms are necessary for this miniaturization trend to continue. The Smart Pebbles (shown in Figure 2) and associated algorithms are a step towards what we believe will be the long legacy of programmable matter.

In this work, we present a new algorithm which helps automated the process of shape formation in large self-assembling modular robotic systems. In a system with millions, or even hundreds of modules, it is time consuming if the user has to decide exactly which modules should be used to form a particular goal shape. It is easy for the user to give the system high level guidance that approximates the user's desires, but computational systems demand exact answers. Our algorithm allows a programmable matter system to automatically determine which of its modules to allocate to the goal shape.

### A. Related Work

This work is based on our prior work with the Pebbles system. It assumes some knowledge of the hardware [1] and shape formation algorithms [2], [3] that we have previously developed. The majority of existing self-assembling systems aim to form structures in one of two ways. Some systems such as [4], [5], [6], [7], [8] use a collection of application specific differentiated modules, that are only capable of assembling in a particular fashion to form a specific shape. In contrast, other systems such as [9], [10], [11], [12], [13], [14], [15], [16] use completely generic modules with more computation and communication ability embedded in each module. Both types of systems aim to form complex shapes in a direct manner: as these structures grow from a single module, new modules are only allowed to attach to the structure in specific locations.

We propose a new approach that eliminates many of the complexities of shape formation by active assembly. As

K. Gilpin and D. Rus are with the Computer Science and Artificial Intelligence Lab, MIT, Cambridge, MA, 02139, [kwgilpin@csail.mit.edu](mailto:kwgilpin@csail.mit.edu), [rus@csail.mit.edu](mailto:rus@csail.mit.edu).

shown in Figure 1, our Smart Pebble system employs a set of distributed algorithms to perform two discrete steps: 1) rely on stochastic forces to self-assemble a close-packed crystalline lattice of modules and 2) use the process of self-disassembly to remove the extra material from this block leaving behind the goal structure. By approaching shape formation in this manner, we hope to speed up the entire process, eliminate any global information that must be distributed throughout the system, and simplify the computing requirements of each module.

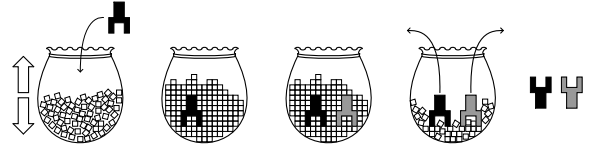


Fig. 1. To form shapes using the Smart Pebbles system, a passive object to be duplicated (shown in black) is submerged in a large collection of programmable matter particles. The particles solidify in a regular lattice to encase the passive shape. Once solidified, modules bordering on the passive shape sense its topology and inform other modules in the vicinity that they will become part of the duplicate shape. Once these duplicate modules (shown in grey) have been notified, all other modules break their mechanical bonds leaving just the original and duplicate shapes behind. When the user is done with the duplicate, he may drop it back into the bag where it will disintegrate, and the modules can be reused.

## II. HARDWARE

As shown in Figure 2, each Smart Pebble is a 12mm cube capable of autonomously communicating with and latching to four neighboring modules in the same plane to form 2D structures. Each completed module weighs 4.0g and may be rotated any one of four ways on the assembly plane and still mate with its neighbors. The major functional components of each module are power regulation circuitry, a microprocessor, and four electropermanent (EP) magnets, which are responsible for latching, power transfer, and communication. While a 3D system is theoretically possible, it would leave little room for electronics inside each module. Additionally, the pole arrangement of the EP magnets would need to be made 8-way or axially symmetric.

## III. SYSTEM OPERATION

Our approach to object formation in the Pebbles system is a two-step process. First, we employ self-assembly (see Figure 3) to automatically pack the modules into a dense lattice structure. During this step, the system has no concept of the ultimate goal shape it will eventually be asked to form. Once the self-assembly step is complete, and all free

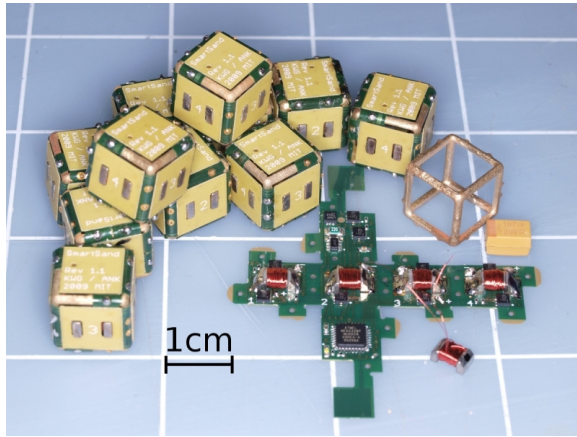


Fig. 2. Each programmable matter pebble is a 12mm per side, and together they are able to form complex 2D shapes using four electropermanent magnets able to hold 85 times the individual module weight. The pebbles are formed by wrapping a flexible circuit around a brass frame. An energy storage capacitor hangs between two tabs occupies the center of the module.

module coalesced into a solid structure, the system starts a controlled disassembly process during which mechanical bonds between neighboring modules are selectively broken. Only the bonds between modules that form the desired goal shape are maintained. When the disassembly process is complete, the user can brush aside the extra modules to reveal the completed object.

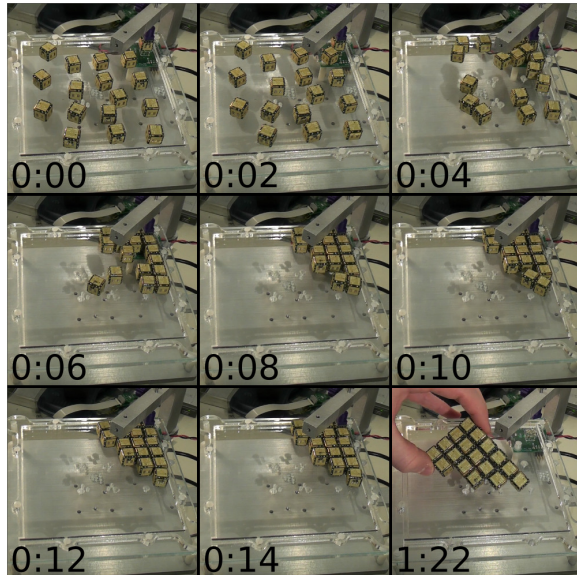


Fig. 3. A collection of 16 randomly distributed Smart Pebble modules, (each a 12mm cube), and one fixed root module, (back right of each video frame), self-assemble when placed on an inclined vibration table. Initially, the connectors on each module are deactivated, and they are only turned on when a module successfully communicates with the growing structure. The last frame shows that all modules bond together to form a solid shape that can then be used for self-disassembly.

By aiming to form a close-packed lattice during the self-assembly phase, we eliminate the need to transmit a description of the goal shape to every module in the structure. Our two-step approach to shape formation attempts to minimize

the amount of information transmitted to modules in the system because it does not transmit a complete blueprint of the structure to all modules. The alternative, in systems that perform self-assembly in a one-step process, is to transmit information to every single module indicating on which faces that module should allow neighbors to bond. This blueprint for the goal object has unacceptable communication and storage costs.

In addition to simplifying communication, the other major advantage of self-assembling a close-packed lattice before self-disassembling into the desired shape is that the modules in the lattice form a supportive scaffolding. The scaffolding adds mechanical rigidity while the goal shape is being formed, and it also helps to better constrain and align modules as they attach to the system. The scaffolding provides more potential routing paths for messages in the system.

Once the system has formed a solid, close-packed block of material, it must be informed of the goal shape. In this work, we will focus on duplication as a means of goal shape description. At the start of the self-assembly process, the user inserts a physical (potentially miniaturized) model of the shape to be formed. This model is incorporated into the growing structure. Then, once self-assembly is complete, the system employs the duplication algorithms to autonomously sense the shape of, and duplicate, the passive object. The advantage of duplication is that we completely eliminate the need for an external controller. This makes the system more practical, and it eliminates the extraordinary communication burden from whatever module would otherwise, serve as the communication link between the system and an external controller.

For details on the core of the duplication algorithm, consult [2], but we present a summary of it here. The duplication process operates by detecting the boundary of the obstacle being duplicated. By routing messages around the perimeter of the obstacle, the algorithm notifies all modules on the boundary of their unique status. Once all of these original border modules are notified, each sends a message (in an agreed upon direction) to a unique module that will become part of the duplicate's border. Once all of the modules on the duplicate shape's border have been notified, we use a flood fill process to notify all modules inside this border that they are part of the duplicate shape. When all other modules in the system start the disassembly, these modules maintain their bonds with the neighbors to that goal shape is formed. Due to the one-to-one correspondence between modules on the border of the original object and the modules on the border of the duplicate shape, the duplicate will be a perfect copy of the original.

#### IV. AUTOMATED DUPLICATION PLACEMENT

This work presents a new algorithm which allows the system to automatically decide where within the initial block of programmable matter to place the duplicate shape. In an automated duplication system with millions of minuscule programmable matter modules, it would be difficult for the user to explicitly instruct the system where to place

the duplicate. Our automated shape placement algorithm eliminates the need for the user to specify where the duplicate should be placed. The automated shape placement algorithm is executed by the obstacle leader between the sensing and border identification steps of the larger distributed duplication process. In short, the algorithm attempts to find the optimal placement of the duplicate object's bounding box within the rectangular bounding box surrounding all modules in the system.

The placement algorithm represents the duplicate object with a rectangular bounding box. As explained above, the shape sensing algorithm learns the size and position of original shape's bounding box by routing a sense (SEN) message around the perimeter of the shape being duplicated. When this sense message returns to the obstacle leader, it contains the bounding box. Figure 4 shows the bounding box of the original shape being duplicated (labeled "O") as a dashed line. A bounding box of the same dimensions will also enclose the duplicate shape that the system is attempting to form. The system must decide where to place the duplicate's bounding box. Figure 4 shows four potential positions for the duplicate (labeled "A" through "D"). The bounding box associated with each potential position is drawn as a dotted line.

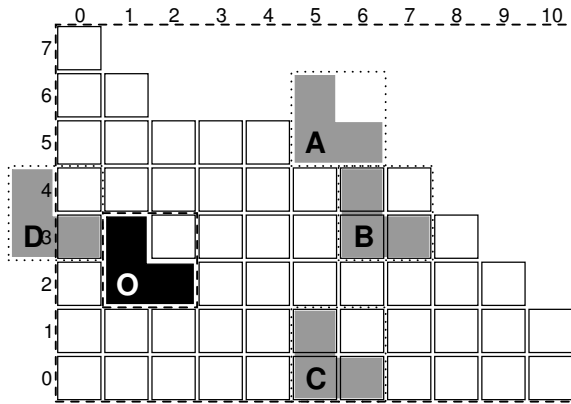


Fig. 4. The automated duplicate placement algorithm attempts to place the duplicate shape as far from the edges of the surrounding block of material as possible. To simplify the optimization, the algorithm uses rectangular bounding boxes, (dashed and dotted lines), to represent both the original shape and the collection of programmable matter modules surrounding it. In this example, the algorithm determines that placement B is ideal.

Modules on the perimeter of the collection of programmable matter modules encasing the shape being duplicated also route sense messages around the perimeter of the collection of modules. We call this two-dimensional collection of communicating modules a *slice*. One of the sense messages traversing the inside perimeter of the slice will eventually return to the *slice leader*, which is the module on the perimeter of the collection of modules with the highest UID. Because it circumnavigated the inside of the slice, (in contrast to the outside of an obstacle), this sense will indicate that the sensed area is negative. The slice leader uses this fact to determine that it is, in fact, the *slice*, not *obstacle*, leader. Despite returning with a negative area, the sense message

that returns to the slice leader holds the position and size of rectangular bounding box surrounding all modules in the system. This bounding box is also represented by a dashed rectangle surrounding all modules in Figure 4.

With both the obstacle's and the slice's bounding boxes known, the automated shape placement algorithm attempts to find the optimal placement of the obstacle's bounding box within the slice's bounding box. To do so, the algorithm instructs the slice leader to broadcast the slice's bounding box to all modules in the system. Because the slice leader does not know the coordinates of the obstacle leader, this is the easiest way to guarantee that the obstacle leader learns the slice's bounding box. Once the obstacle leader receives the message containing the slice's bounding box, it considers four distinct placements of the duplicate shape. In particular, the obstacle leader considers placing the duplicate shape in the four cardinal directions relative to the original shape's location. Starting to the north, and moving clockwise, the obstacle leader considers placements A through D in Figure 4.

Determining the optimal placement is a two step process. First, for each cardinal direction, the algorithm determines if the duplicate has any chance of fitting between the original shape's bounding box and the slice's bounding box. In the example of Figure 4, the algorithm determines that placements A, B, and C are all potential candidates. It eliminates placement D because the duplicate's bounding box is two modules wide, but the space between the left side of the original's bounding box and the slice's bounding box is only one module wide.

Second, having eliminated cardinal directions that it knows will not fit the duplicate, the obstacle leader attempts to find the optimal placement among the remaining directions. For each direction, the algorithm attempts to center the duplicate's bounding box in both the x- and y-directions. For example, when attempting to place the duplicate north of the original, the algorithm attempts to center the duplicate between the top edge of the original's bounding box and the top edge of the slice's bounding box. Simultaneously, the algorithm attempts to center the duplicate between the left and right edges of the slice's bounding box.

The algorithm scores each potential placement. The score is the sum of the extra space surrounding the duplicate object. Returning to our example in Figure 4, the score associated with placement A is 11. This score comes from the 1 module of space above, 4 modules to the right, 5 modules to the left, and 1 module below the duplicate. The reason placement A is only credited with 1 module of space below is that the algorithm measures the distance between the bottom of the duplicate and the top of the original shape. It assumes that the original shape may extend farther to the right than it actually does. The scores for all placements are shown in Table I. Ultimately, placement B is declared optimal with a score of 12.

While the automated shape placement algorithm we describe makes some attempt at optimality, it is not ideal. While it just happens to be the case that placement B in Figure 4

TABLE I

THE AUTOMATED PLACEMENT ALGORITHM CHOOSES THE VIABLE POSITION WITH THE HIGHEST SCORE. FOR REFERENCE, CONSULT FIGURE 4.

Cardinal Dir.	Placement	Viable	Score
North	A	Yes	11
East	B	Yes	12
South	C	Yes	9
West	D	No	n/a

results in an accurate copy of the original being formed, all of the modules that will be used to build that duplicate could be removed without affecting the algorithm's decision to place the duplicate at position B. This shortcoming is due to the fact that the algorithm uses rectangular bounding boxes to represent more complex shapes. A simple bounding box cannot capture the fact that there are many modules missing from the upper right in Figure 4. Additionally, the algorithm fails to account for any modules missing from the interior of the structure. These non-idealities are the result of a calculated decision. If we used more complex data structures to describe the shape of the obstacle and slice, the communication, storage, and computation costs would rise. For an arbitrarily complex slice, containing an arbitrarily complex object to be duplicated, we would need  $O(n)$  bits of storage to determine the optimal placement. We have chosen rectangular bounding boxes because they only require  $O(1)$  space, and they make the optimal placement calculations easy and fast.

We have not extended the algorithm to scenarios in which we wish to magnify the original or create multiple copies, but this task should not be difficult. For example, instead of using an exact replica of the original's bounding box to place the duplicate, we could use a modified bounding box to describe the duplicate object(s). The algorithm could simply magnify or replicate the original shape's bounding box to create the duplicate's bounding box. It could then use this larger bounding box during the optimization process.

## V. DISCUSSION

While this work has not addressed all of the algorithmic challenges associated with miniaturizing programmable matter systems, it has attempted to solve the problem of automating goal shape placement in a large array of modules. In the future, we hope to expand this work to three dimensions. Additionally, we are investigating the use of more intricate shape abstractions so that we do not have to represent the object and the surrounding material with simple rectangles. The key will be to choose flexible representation so that the time and communication costs can be tailored to the resources available.

## VI. ACKNOWLEDGMENTS

This work is supported by the US Army Research Office under grant number W911NF-08-1-0228, the NSF through Grants 0735953, 1138967, and 1240383, and the NDSEG fellowship program.

## REFERENCES

- [1] K. Gilpin, A. Knaian, and D. Rus, "Robot pebbles: One centimeter robotic modules for programmable matter through self-disassembly," in *IEEE International Conference on Robotics and Automation (ICRA)*, May 2010.
- [2] K. Gilpin and D. Rus, "A distributed algorithm for 2d shape duplication with smart pebble robots," in *IEEE International Conference on Robotics and Automation (ICRA)*, 2012, p. In Press.
- [3] ———, "What's in the bag: A distributed approach to 3d fabrication by duplication with modular robots," in *Robotics Science and Systems (RSS)*, July 2012.
- [4] S. Miyashita, M. Kessler, and M. Lungarella, "How morphology affects self-assembly in a stochastic modular robot," in *IEEE International Conference on Robotics and Automation*, May 2008, pp. 3533–3538.
- [5] M. Shimizu and K. Suzuki, "A self-repairing structure for modules and its control by vibrating actuation mechanisms," in *IEEE International Conference on Robotics and Automation (ICRA)*, May 2009, pp. 4281–4286.
- [6] P. W. K. Rothemund and E. Winfree, "The program-size complexity of self-assembled squares," in *32rd Annual ACM Symposium on Theory of Computing*, 2000, pp. 459–468.
- [7] L. Adleman, Q. Cheng, A. Goel, and M.-D. Huang, "Running time and program size for self-assembled squares," in *33rd Annual ACM Symposium on Theory of Computing*, 2001, pp. 740–748.
- [8] G. Aggarwal, M. H. Goldwasser, M.-Y. Kao, and R. T. Schweller, "Complexities for generalized models of self-assembly," in *15th Annual ACM-SIAM Symposium on Discrete Algorithms*, 2004, pp. 880–889.
- [9] J. Bishop, S. Burden, E. Klavins, R. Kreisberg, W. Malone, N. Napp, and T. Nguyen, "Programmable parts: A demonstration of the grammatical approach to self-organization," in *IEEE/RSJ International Conference on Intelligent Robots and Systems (IROS)*, August 2005, pp. 3684–3691.
- [10] N. Napp, S. Burden, and E. Klavins, "The statistical dynamics of programmed self-assembly," in *IEEE International Conference on Robotics and Automation (ICRA)*, May 2006, pp. 1469–1476.
- [11] P. White, K. Kopanski, and H. Lipson, "Stochastic self-reconfigurable cellular robotics," in *IEEE Conference on Robotics and Automation*, April 2004, pp. 2888–2893.
- [12] P. White, V. Zykov, J. Bongard, and H. Lipson, "Three dimensional stochastic reconfiguration of modular robots," in *Robotics Science and Systems*, June 2005.
- [13] M. Tolley, J. Hiller, and H. Lipson, "Evolutionary design and assembly planning for stochastic modular robots," in *IEEE Conference on Intelligent Robotics and Systems (IROS)*, October 2009, pp. 73–78.
- [14] C. Jones and M. J. Matarić, "From local to global behavior in intelligent self-assembly," in *IEEE International Conference on Robotics and Automation (ICRA)*, 2003, pp. 721–726.
- [15] J. Kelly and H. Zhang, "Combinatorial optimization of sensing for rule-based planar distributed assembly," in *IEEE International Conference on Intelligent Robots and Systems*, 2006, pp. 3728–3734.
- [16] J. Werfel, "Ant hills built to order: Automating construction with artificial swarms." Ph.D. dissertation, Massachusetts Institute of Technology, 2006.

# Addressing of Micro-Robot Teams and Non-Contact Micro-Manipulation

Eric Diller, Zhou Ye, Joshua Giltinan and Metin Sitti

**Abstract**—We present two methods for the addressable control of multiple magnetic microrobots. Such methods could be valued for microrobot applications requiring high speed parallel operation. The first uses multiple magnetic materials to enable selective magnetic disabling while the second allows for independent magnetic forces to be applied to a set of magnetic micro-robots moving in three dimensions. As an application of untethered magnetic microrobots, we also present a non-contact manipulation method for micron scale objects using a locally induced rotational fluid flow field. The micro-manipulator is rotated by an external magnetic field in a viscous fluid to generate a rotational flow field, which moves the objects in the flow region by fluidic drag. Due to its untethered and non-contact operation, this micro-manipulation method could be used to quickly move fragile or non-fragile micro-objects in inaccessible or enclosed spaces such as in lab-on-a-chip devices.

## I. INTRODUCTION

The control of multiple micro-robots could have a major impact to enable parallel and distributed operation for manipulation, distributed sensing and other tasks in inaccessible micro-scale spaces. Micro-robots controlled and powered using magnetic fields have gained use recently because they can be controlled remotely using relatively large magnetic forces and torques, can be a bio-compatible actuation method, and they can often be fabricated simply [1,2]. However, methods to control teams of magnetic microrobots have been limited in the literature to crawling on planar surfaces [3,4], and have issues of scalability. Here we present two new methods for the independent control of magnetic micro-robot teams. The first method uses composites of two magnetic materials to achieve on/off magnetization of individual micro-robots. By controlling the states of each agent, control over the set is achieved. This method is scalable to large arrays of micro-robots. The second addressing method achieves multi-robot control for micro-robots levitating in a liquid medium for three-dimensional (3D) motion. Such 3D independent control has not been shown before, and is here accomplished by designing each micro-robot to respond uniquely to the same input magnetic fields.

Micro-object manipulation has wide potential applications in microfluidics, biological and colloidal science, lab-on-a-chip systems, and micro-assembly for systems such as micro-optical electro mechanical systems. Various techniques have been developed to achieve micro-manipulation in different backgrounds. These techniques can be categorized into two groups, contact-based manipulation and non-contact-based manipulation. Micro-grippers are

major member of the first type [5,6], while externally controlled bacteria also fall into this group [7]. Many untethered micro-robots can also achieve manipulation tasks using mechanisms in the first category [8-10]. The second category includes optical tweezers [11], magnetic tweezers [12], dielectrophoresis [13], electrophoresis [14], optical arrays, and microfluidic devices, including use of micro-pumps/valves or magnetophoresis. Non-contact manipulation has also been implemented with several untethered micro-manipulators [15,16].

We present a non-contact micro-object manipulation method using a locally induced rotational fluid flow field created by an untethered spherical magnetic micro-manipulator. The magnetic micro-manipulator is rotated in a viscous fluid by an externally generated magnetic field to create a rotational flow, which propels micro-objects in the flow region. One single spherical micro-manipulator is used to handle one object at a time. Automated manipulation of micro-beads is implemented based on visual feedback, with a very precise object position error of less than 20% of the object size.

## I. MULTI-ROBOT CONTROL USING DISABLING MAGNETISM

### A. Disabling by Magnetic Hysteresis

Remotely and selectively turning on and off the magnetization of many micro-scale magnetic actuators could be a great enabling feature in fields such as microrobotics and microfluidics. We have developed an array of addressable sub-mm micro-robots made from a composite material whose net magnetic moment can be selectively turned on or off by application of a large magnetic field pulse. The material is made from a mixture of micron-scale neodymium-iron-boron and ferrite particles, and can be formed into arbitrary actuator shapes using a simple molding procedure.

To achieve many-state magnetic control of a number of microrobotic actuators, we require a number of magnetic materials with different hysteresis characteristics. The magnetic coercivity and remanence (retained magnetization value when the applied field  $H$  is reduced to zero) for commonly-used materials vary over several orders of magnitude. These materials cover a wide range of hysteresis values, from NdFeB and SmCo, which are permanent under all but the largest applied fields, to iron, which exhibits almost no hysteresis. For comparison, the magnetic fields applied to actuate magnetic microactuators are typically smaller than 12 kA/m, which is only strong enough to remagnetize iron. Thus, the magnetic states of SmCo, NdFeB, ferrite and alnico can be preserved when driving an actuator. This can be used to independently control the magnetization of each material, even when they share the

The authors are with the Department of Mechanical Engineering, Carnegie Mellon University, Pittsburgh, PA USA. (e-mail: sitti@cmu.edu).

same workspace. By applying a pulse in the desired direction greater than the coercivity field ( $H_c$ ) of a particular material, an independent magnetization state of each magnet material can be achieved instantly.

In general it is difficult to demagnetize a single magnet by applying a single demagnetizing field because the slope of the hysteresis loop (i.e. the magnetic permeability) near the demagnetized state is very steep. Thus, such a demagnetization process must be very precise to accurately demagnetize a magnet. While steadily decreasing AC fields can be used to demagnetize a magnetic material, this method does not allow for addressable demagnetization because it will disable all magnets in the workspace. This motivates the use of a magnetic composite to enable novel untethered addressable magnetic disabling.

We employ a different demagnetization procedure to achieve a more precise demagnetization by employing two materials, both operating near saturation where the permeability is relatively low. In this method, an applied switching field  $H_{pulse}$  can be applied to switch only one material's (ferrite in this example) magnetization without affecting the second material (NdFeB). This switching allows the device to be switched between on and off states as the magnetic moments add in the on state or cancel in the off state. While the internal field of the magnet at any point will not be zero, the net field outside the magnet will be nearly zero, resulting in negligible net magnetic actuation forces and torques.

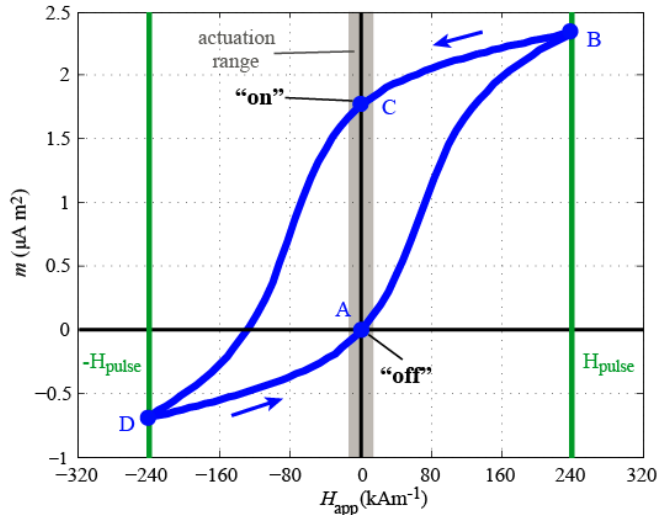


Figure 1. The  $H$ - $m$  hysteresis loop of a composite microrobot made from ferrite and NdFeB. A 240 kA/m, field switches the ferrite magnetization while leaving the NdFeB unaffected, resulting in a vertically-biased loop intersecting the origin, showing clear on and off states.

When fields are applied below the NdFeB coercivity, the NdFeB acts as a permanent magnet, biasing the device magnetization, as shown in the  $H$ - $m$  loop of Fig. 1 for  $H_{pulse}$  up to about 240 kA/m. Traversing the hysteresis loop, the device begins in the off state at point A, where motion actuation fields, indicated by the 12 kA/m range, only magnetize the device to about  $0.08 \mu\text{Am}^2$ , resulting in minimal motion actuation. To turn the device on, a 240 kA/m pulse is applied in the forward direction, bringing the device to point B. After the pulse, the device returns to point C, in

the on state. Here, motion actuation fields vary the device moment between about 1.7 and  $1.8 \mu\text{Am}^2$ . To turn the device off, a pulse in the backward direction is applied, traversing point D, and returning to the off state at point A at the conclusion of the pulse. For small motion actuation fields in the lateral direction, the device is expected to show even lower permeability in the on or off state due to the shape anisotropy induced during the molding process.

### B. Addressable Control Results

A six-electromagnetic-coil system is used to generate the magnetic field required to actuate and control the magnetic micro-manipulator. The system consists of three pairs of air-core independent electromagnetic coils, aligned to the faces of a cube approximately 8.2 cm on a side. A maximum magnetic field of 5 mT can be generated in the workspace, with 6% uniformity over a 30 mm space. The presented disabling method for mobile microrobots can be used to selectively disable multiple microrobots. Based on its orientation when the pulse is applied (and independent of its position), each microrobot will be enabled or disabled. Four and six microrobots are moved using stick-slip motion on a glass slide surface in a viscous oil environment. The viscous fluid environment is provided here to increase the fluid drag to retain microrobot orientation during the pulse. The experimental workspace is placed inside the coil system, allowing for both stick-slip motion on the 2D surface using small magnetic fields up to 2.4 kA/m and magnetic state changes by a larger field pulse. Independent addressing of the on and off states of each microrobot is accomplished by  $H_{pulse}$  applied in-plane.

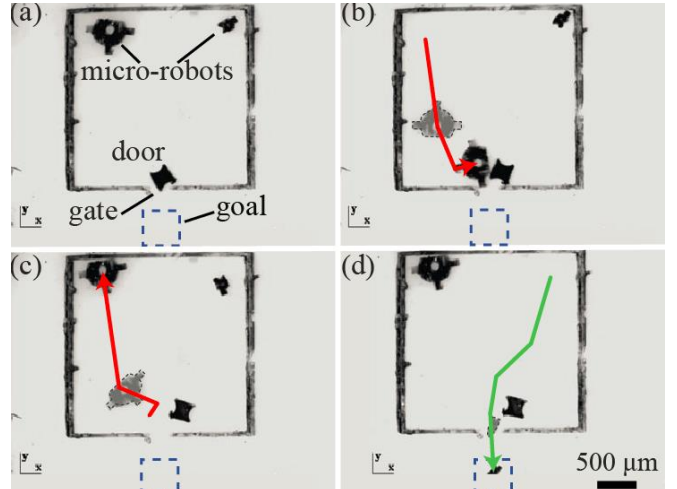


Figure 2. Addressable microrobot teamwork task, requiring the cooperative contribution of two mobile microrobots of different sizes working together to reach a goal. Frames each show two superimposed images, with the microrobot paths traced. (a) Both microrobots lie inside an enclosed area with the door to the goal blocked by a plastic door. Only the larger microrobot can move the door, while only the smaller microrobot is small enough to fit through the gate. (b) The larger microrobot removes the door while the smaller disabled microrobot remains in place. (c) The larger microrobot returns to its starting point and is disabled. (d) The smaller microrobot is enabled and is free to move through the gate to the goal.

An example of two micro-robots accomplishing a teamwork task is shown in Figure 2. Here, the task requires both a strong micro-robot to move the door and a small micro-robot to reach the goal through the small gate. Such a

task is representative of complex tasks in micro-assembly and micro-transport which could benefit from heterogeneous groups of micro-robots.

## II. ADDRESSABLE MICRO-ROBOTS IN 3D

### A. Concept

As a second addressing method for magnetic microrobots which is capable of operation in 3D, we present the first microrobot addressing method for 3D motion control, which works by magnetic gradient pulling. This method allows for completely independent and uncoupled net forces to be applied to each microrobot and thus allows for feedback position control of several microrobots in 3D.

The application of different magnetic forces to each microrobot is accomplished by controlling the unique viscous drag and magnetic torque on each unique microrobot when placed in a rotating magnetic field. The different rotational responses of the geometrically and magnetically distinct designs result in each microrobot assuming a unique orientation in space. Thus, if each microrobot possesses a different magnetic strength or rotational fluid drag coefficient, arbitrary forces could be exerted on each independently and simultaneously using magnetic field gradients, when averaged over one short field cycle. The lag of a permanent magnet microrobot in a spinning magnetic field is determined by the balance between the applied magnetic torque and the drag torque. Fluid flow at the micro-scale is dominated by viscous forces as opposed to inertial forces, with typical Reynolds numbers of 0.01 or lower for the microrobot size scales around or smaller than 1 mm.

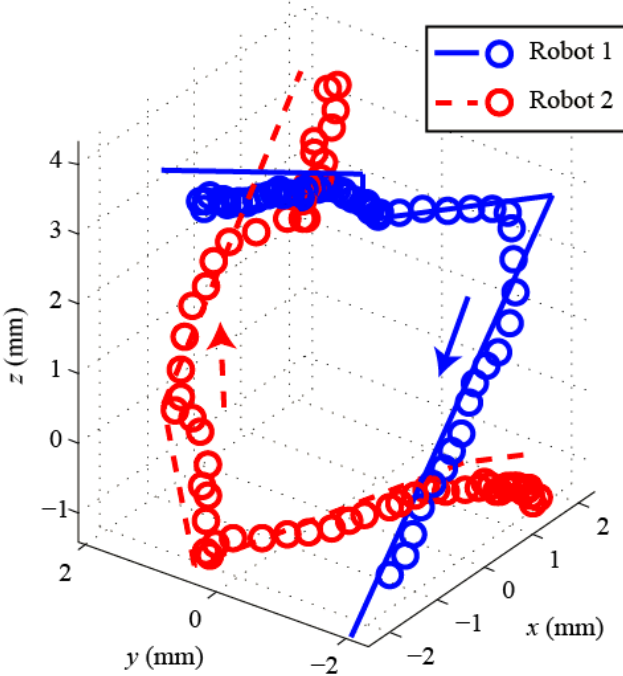


Figure 3. Feedback control for two microrobots following the desired 3D paths in silicone oil with a viscosity of 0.052 Pa s. Circles show the tracked microrobot position every 1.0 s.

### B. Demonstration

An electromagnetic-coil system is used to generate the magnetic fields required to actuate and control the magnetic micro-robots. The system consists of eight coils which are aligned pointing to a common workspace center point with an approximate opening size of 12 cm. A maximum magnetic field of about 20 mT can be generated in the workspace, with 6% uniformity over a 30 mm space.

The feedback control methods are tested experimentally to prove their performance. Control using visual feedback is used to follow desired paths in 3D. Two micro-robots are moved along independent trajectories in 3D space in Figure 3. Here, the microrobots are controlled using the constant field rotation waveform, with a field rotation rate of 1.2 Hz.

## III. NON-CONTACT MICRO-MANIPULATION

The magnetic micro-manipulators used in this study are fabricated via a soft-lithography-based micro-molding process. Small drops of solder are dropped into water to form the positive shapes for the spherical micro-manipulators, ranging from 10  $\mu$ m to 1000  $\mu$ m. The desired sizes are selected from the batch of solder spheres. These selected solder spheres are glued to a glass substrate using a UV curable epoxy (Loctite 3761) and a mold-making elastomer (PDMS, Dow Corning HS II RTV) is poured over to form a negative mold. A mixture of neodymium-iron-boron (NdFeB) particles (Magnequench MQP-15-7) suspended in polyurethane (TC-892, BJB Enterprises) matrix is poured into the negative rubber mold and allowed to cure into the final micro-manipulator shapes.

Experiments are carried out in a 30 mm x 30 mm x 1 mm open-top container filled with silicone oil with a kinematic viscosity of 50 cSt to create a low Re environment. The spherical magnetic micro-manipulators used in all the experiments have a diameter of 360  $\mu$ m, and the objects being manipulated are polystyrene beads with a diameter of 200  $\mu$ m and a density of 1.05 g/cm<sup>3</sup>.

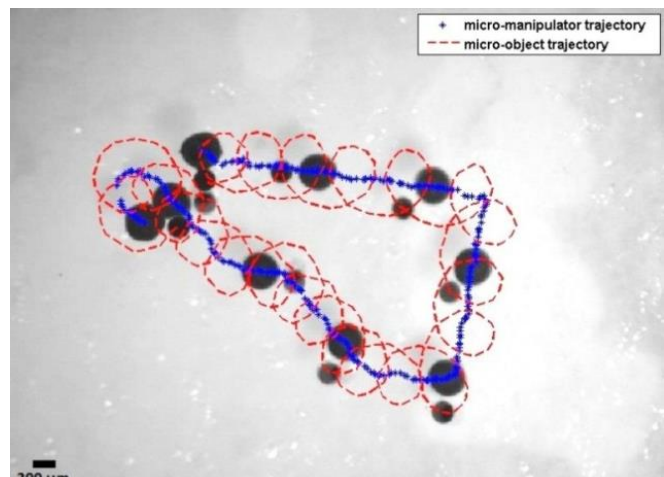


Figure 4. Top-view optical microscope images of a 360  $\mu$ m diameter spherical magnetic micro-manipulator carrying a 200  $\mu$ m diameter polymer micro-bead along an arbitrary path on a glass substrate using rotational fluid field. Eight frames taken from video of the whole manipulation process, with an equal interval of 1.23 s between each of them, are overlaid to show the paths of the micro-manipulator and polymer bead. The entire duration is 9.87 s. The magnetic micro-manipulator rotates at 30 Hz and translates at a speed of approximately 2.5 manipulator-diameters per second (900  $\mu$ m/s).

The capabilities of rotational micro-manipulator locomotion and non-contact micro-object manipulation are shown in Figure 4, where a magnetic micro-manipulator transports a micro-bead on a glass substrate. An external magnetic field with strength of 3.5 mT rotating at a frequency of  $f = 30$  Hz is applied to induce synchronous rotation with the applied field. In this experiment, the rotation axis angle is kept small ( $<10^\circ$  from vertical), resulting in a translational manipulator speed of approximately 5 manipulator-diameters per second ( $\sim 900 \mu\text{m/s}$ ).

Automated coarse/fine manipulation of a 200  $\mu\text{m}$  micro-object is also implemented based on visual feedback, with results illustrated in Figure 5. First, the micro-manipulator slowly rolls from the initial position to the standby position close to the micro-object (Figure 5 (a-b)). Then it starts spinning at a high frequency ( $f = 30$  Hz), picks up the micro-object (Figure 5 (c)) and carries it quickly towards the target position (Figure 5 (d)). The micro-manipulator stops rapid spinning when it gets close to the target position (Figure 5 (e)). To precisely place the micro-object to the target position, the micro-manipulator spins at a low frequency ( $f = 6$  Hz) and slowly pushes the object to the target (Figure 5 (f)). The final average position error is less than 20% of the object size.

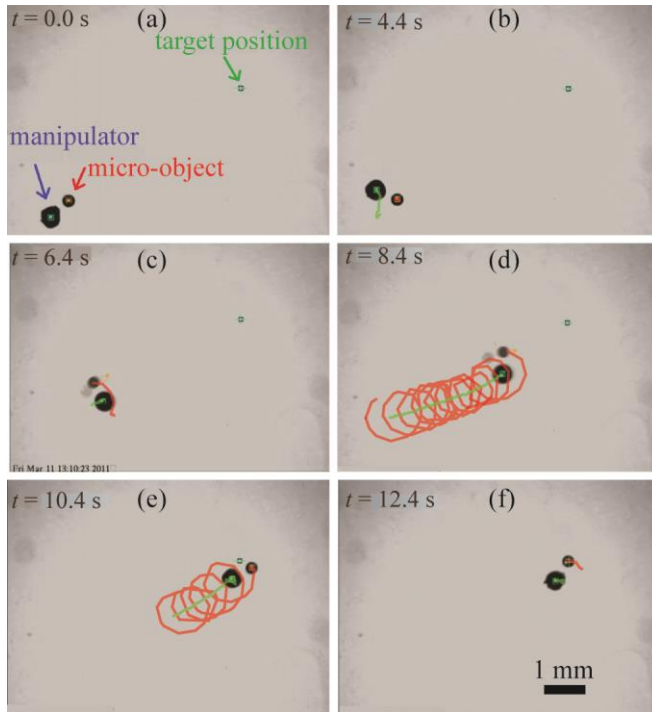


Figure 5. Automated manipulation of a 200  $\mu\text{m}$  diameter polystyrene microbead using a 360  $\mu\text{m}$  diameter spherical magnetic micro-manipulator. Five frames are taken from video of the whole manipulation process at different periods. (a) Initial position. (b) The micro-manipulator slowly rolls to the standby position. (c-d) The micro-manipulator fast spins to pick up and carry the micro-object to the target position. (e) It stops spinning when getting close to the target position, then (f) spins slowly to precisely push the micro-object to the target position.

In conclusion, we have presented two methods for the addressable control of multiple magnetic micro-robots in 2D and 3D. The first method has been shown to be scalable to larger groups of microrobots, while the second method has

achieved multi-robot control in 3D fluid environments. Overcoming such limitations could allow for micro-robot teams to be used in high-impact parallel manipulation tasks. As an application for untethered micro-robots, we then propose using highly mobile rotating magnetic micro-robots to manipulate micro-objects via induced fluid flow at low Reynolds numbers. This method has promise to be a fast and precise non-contact object manipulation scheme for microfluidic environments. This method could benefit from multiple micro-robots working in parallel for high-speed team manipulation.

## REFERENCES

- [1] M. P. Kummer, J. J. Abbott, B. E. Kratochvil, R. Borer, A. Sengul, and B. J. Nelson, "OctoMag: An electromagnetic system for 5-DOF wireless micromanipulation," *IEEE Transactions on Robotics*, vol. 26, no. 6, pp. 1006–1017, 2010.
- [2] C. Pawashe, S. Floyd and M. Sitti, "Modeling and experimental characterization of an untethered magnetic micro-robot," *International Journal of Robotics Research*, vol. 28, pp. 1077-1094, 2011.
- [3] E. Diller, S. Floyd, C. Pawashe, and M. Sitti, "Control of Multiple Heterogeneous Magnetic Microrobots in Two Dimensions on Nonspecialized Surfaces," *IEEE Transactions on Robotics*, vol. 28, no. 1, pp. 172–182, 2012.
- [4] E. Diller, C. Pawashe, S. Floyd, and M. Sitti, "Assembly and disassembly of magnetic mobile micro-robots towards deterministic 2-D reconfigurable micro-systems," *The International Journal of Robotics Research*, vol. 30, no. 14, pp. 1667–1680, Sep. 2011.
- [5] M. Carrozza, P. Dario, A. Menciassi and A. Fenu, "Manipulating biological and mechanical micro-objects using LIGA-microfabricated end-effectors," *IEEE International Conference on Robotics and Automation*, pp. 1811-1816, 1998.
- [6] D. Kim, B. Kim and H. Kang, "Development of a piezoelectric polymer-based sensorized microgripper for microassembly and micromanipulation," *Microsystem Technologies* vol. 10, pp. 275-280, 2004.
- [7] S. Martel, C. Tremblay, S. Ngakeng and G. Langlois, "Controlled manipulation and actuation of micro-objects with magnetotactic bacteria," *Applied Physics Letters*, vol. 89, 233904, 2006.
- [8] B. Behkam and M. Sitti, "Bacterial flagella-based propulsion and on/off motion control of microscale objects," *Applied Physics Letters*, vol. 92, 223901, 2008.
- [9] S. Tottori, L. Zhang, F. Qiu, K. K. Krawczyk, A. Franco-Obregón and B. J. Nelson, "Magnetic helical micromachines: fabrication, controlled swimming, and cargo transport," *Advanced Materials*, vol. 24, pp. 811-816, 2012.
- [10] D. Grier, "A revolution in optical manipulation," *Nature* vol. 424, pp. 810-816, 2003.
- [11] J. Yan, D. Skoko and J. Marko, "Near-field-magnetic-tweezer manipulation of single DNA molecules," *Physical Review E*, vol. 70, 011905, 2004.
- [12] P. Chiou, A. Ohta and M. Wu, "Massively parallel manipulation of single cells and microparticles using optical images," *Nature*, vol. 436, pp. 370-372, 2005.
- [13] L. Kremser, D. Blaas and E. Kenndler, "Capillary electrophoresis of biological particles: viruses, bacteria, and eukaryotic cells," *Electrophoresis*, vol. 25, 2282-2291, 2004.
- [14] T. Petit, L. Zhang, K. E. Peyer, B. E. Kratochvil and B. Nelson, "Selective trapping and manipulation of microscale objects using mobile microvortices," *Nano Letters*, vol. 12, pp. 156-160, 2011.
- [15] Z. Ye, E. Diller and M. Sitti, "Micro-Manipulation Using Rotational Fluid Flows Induced by Wireless Magnetic Micro-Manipulators," *Journal of Applied Physics*, vol. 112, no. 6, 064912, 2012.

# Tubular nanojet engines: smart design for smart nanorobots\*

Samuel Sánchez, Wang Xi, Alexander A. Solovev, Oliver G. Schmidt

**Abstract**— We designed nanoscale tools in the form of autonomous and remotely guided catalytically and magnetically self-propelled micro- and nanotools containing sharp tips that can be applied for mechanical drilling operations of biomaterials (fixed HeLa cells and tissues) *ex vivo*.

## I. INTRODUCTION

The mimicry of mechanized macroscale functions at the nanoscale is important for nanomanufacturing and nanorobotics. However, even simple macroscopic tasks are extremely challenging at these small size scales, since it is hard to achieve and control nanoscale actuation reproducibly, reversibly and especially in a wireless manner.

The creation and implementation of dynamic micro- and nanoscale mechanized structures with advances in micro/nanotechnology are believed to revolutionize minimally invasive surgery (MIS). The first step towards enabling this vision is to create small tools that can mimic the functionality of larger tools utilized in surgery [1]. In addition, it is necessary to develop methods so that these tools can be guided and implemented in a tether-free manner. One class of tools in surgery is the sharp surgical instruments that are widely utilized for making incisions. Some of these surgical instruments are enabled by electromagnetic motors on the macroscale, but it can be very challenging to harness the energy in a tether-free manner required to perform drilling at smaller size scales.

One approach to power micro- and nanoscale tools involves the catalytic conversion of chemical energy (energy-rich molecules in solution) into mechanical energy [2]. Catalytically constituted micro- and nano- structures can accelerate the decomposition of hydrogen peroxide and enable the self-propulsion of micro- and nanomotors, pumping of fluids, and transport of colloidal particles and cells [2d-f].

Such miniaturized and remote-controlled microtools may have high potential for *in vivo* applications in the near future in the circulatory, the urinary and the central nervous systems [3]. However, to fabricate cost-effective and operative MIS devices, scientists need to make use of fabrication techniques that enable mass production of non-trivially shaped three dimensional structures, often with multiple classes of materials [4]. In this context, rolled-up

nanotechnology –previously envisioned for nanodriller applications [5]– meets the above described requirements.

## II. RESULTS AND DISCUSSION

We fabricated catalytic tubes with diameters in the sub-micrometer range and investigated control over their catalytic motion. By using molecular beam epitaxy (MBE), thin films of InGaAs/GaAs were deposited on sacrificial AlAs layers and bulk GaAs substrate, and a thin catalytic Pt film sputtered on top. By rolling up those nanomembranes, we fabricated catalytic nanotubes with diameters approximately 20 times smaller than previously reported rolled-up microjets [6] and half the size of the recently designed nanojets [7]. Consequently, we reported the smallest man-made catalytic jet engines.

### A. Catalytic Nanojets drilling into fixed cells[1c]

The catalytic nanojets are powered by the decomposition of H<sub>2</sub>O<sub>2</sub> into molecular oxygen which accumulates in the small cavity and eventually gets released from one end of the nanotube as visible bubbles (Fig. 1). Fig. 1 illustrate the motion and trajectories of InGaAs/GaAs/Cr/Pt (3/3/1/1 nm) nanojets immersed in peroxide fuel. These results demonstrate that bubble driven catalytic nanojets can indeed overcome Brownian diffusion as well as the high viscous forces of the fluid at low Reynolds numbers. We can intentionally design their structure so that many of the fabricated nanotubes present a sharp tip, clearly seen in Fig. 1 and Fig 2A (b-c). The release of bubbles from these rolled-up structures is asymmetric in nature, thus the catalytic nanojets move in different trajectories, including corkscrew fashion (Fig 1A).

We exploited the corkscrew propulsion (Fig 1A) of the nanojets to drill into biomaterials such as those constituting Hela cells, which are an immortal cell line derived from cervical cancer. It should be noted that we utilized paraformaldehyde to fix the cells prior to the drilling experiments for two reasons: [1c]

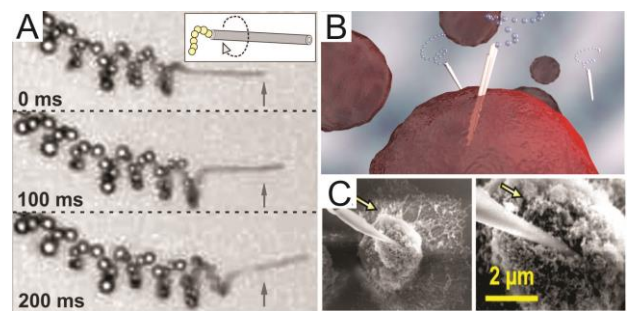


Figure 1. (A) Corkscrew-like motion of a rolled-up microjet. Schematic (B) and SEM images (C) of a rolled-up microjet embedded into cells.

\*Research supported by VW Foundation and the European Research Council.

Institute for Integrative Nanosciences, IFW Dresden, Helmholtzstr. 20, D-01069 Dresden, Germany

[s.sanchez@ifw-dresden.de](mailto:s.sanchez@ifw-dresden.de)

O. G. Schmidt also at Material Systems for Nanoelectronics, Chemnitz Technical University, Reichenhainer Strasse 70, 09107 Chemnitz, Germany

(a) we wanted to remove the influence of any chemically induced deformation of the cell during drilling in the H<sub>2</sub>O<sub>2</sub> fuel, (b) These fixed cells represent a cross-linked version of a realistic cellular biomaterial, so we rationalized that if the nanotools could generate enough force to drill into fixed cells, they would likely have more than enough force to drill into un-cross-linked cells. The type of motion needed for drilling is clearly shown in Fig. 1 by optical microscope sequences of an individual nanojet which self-propels in a screw-like motion during 200 ms at a rotational frequency of 10 Hz (fuel composition: 20 % v/v H<sub>2</sub>O<sub>2</sub>, 10 % v/v surfactant). Straight arrows in the images indicate the linear displacement of the nanojet during the studied time. The inset of Fig. 1A depicts a schematic of the rotation of the nanojet during translation. The schematic image in Fig. 1B displays nanotools which self-propel and embeds itself into a fixed Hela cells. Once the cellular boundary is reached, the nanotools stick to it and start drilling into the cellular biomaterial over several minutes (Fig. 1C).

Although the fuel employed for self-propulsion is still toxic to sustain viable mammalian cellular functions, alternative mechanisms of powered motion and working conditions foresee the use of this concept in diverse applications such as biomedical engineering, biosensing and biophysics. While hydrogen peroxide may be acceptable for applications in nanomanufacturing and nanorobotics, biocompatible fuels need to be developed for live-cell applications. Nonetheless, due to the reduced dimensions but yet the high propulsion power, our results suggest strategies of using shape, size and asymmetry of catalytic nanostructures as tools to realize mechanized functions at the nanoscale.

#### B. Fuel Free Micro-drillers into tissues ex-vivo [8]

To circumvent the limited applications of toxic fuel in vivo, an attractive approach relies on the fabrication of “fuel-free”, e.g. those powered by external magnetic fields. Recently, the enzymatically-triggered and tetherless thermobiochemical actuation of miniaturized grippers and tools, magnetically guided into liver tissues, was demonstrated. [1a,b]

With the same rolled-up technology, we fabricated tubular Ti/Cr/Fe micro-drillers containing sharp tips (Fig 2A) that can be applied for mechanical drilling operations of porcine liver tissue *ex vivo* (Fig. 2B). An external rotational magnetic field is used to remotely locate and actuate the micro-drillers in a solution with a viscosity comparable to that of biological fluids (e.g., blood). Changes in the frequency of the rotating magnetic field results in the switching of the rotational orientation of the micro-driller from a horizontal to a vertical one, which lifts the tubes and makes them suitable for drilling purposes. When microtools are place on hard planar surfaces (e.g. glass or silicon) and re-orient to the upright rotation, they are able to “walk” towards the center of the rotational magnetic field.

To demonstrate the drilling operation (Fig. 2B), a pig liver section was placed at the centre of the magnetic field in a petri dish containing microtools in the working solution (soap-water, 50 % (v/v)). The angular frequency was

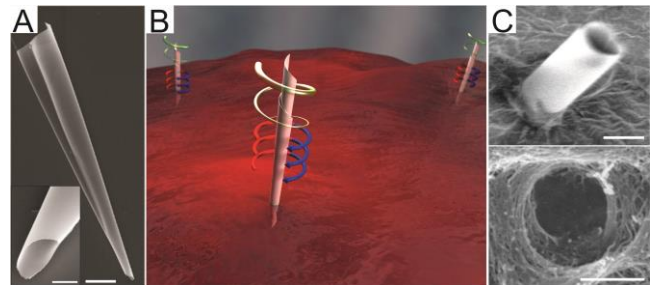


Figure 2. Magnetic microdrillers. A) SEM images of a sharp microtube. B) Schematic of the motion and drilling of microtubes into tissues *ex-vivo* using rotating magnetic field. C) (upper panel) SEM image of a microdriller embedded into the pig liver section after drilling; (lower panel) SEM image showing the drilled hole in the pig liver section after extracting the microdriller by a strong permanent magnet (500 mT). Scale bar: 1 μm in (A), 5 μm in (B) and (C).

increased to 1150 rpm at which the microtools switched their orientation from horizontal into vertical one. Thereafter, the microtools were guided to the desired locations and start the drilling operation from tens of minutes to few hours. It was observed that the microtools retain upright orientation and the initial rotation frequency (~1150 rpm) immediately after reaching the tissue, but significantly slowed down in rotation frequency to few hundreds rpm (~400 rpm) after several minutes standing on the tissue. However, that is not the case for microtools rotating on rigid glass surface, where they rotate at frequencies similar to the applied external rotation field (~1150 rpm).

Using these micro-drillers, we show that magnetic rolled-up microtubes can be used for directed drilling holes in soft matter using porcine liver tissue as a model system.

#### III. CONCLUSION

We demonstrated the fabrication of 3D ferromagnetic microdrillers with sharp tips for drilling operation of soft biomaterials. The rolled-up microtools were formed from 2D nanomembranes of trapezia geometry. It is possible to dynamically switch the orientation of the microtool from a horizontal to a vertical position by changing the frequency of the external processing magnetic field and the viscosity of the solution. We presented magnetic control, drilling and guidance of fuel free microtools toward tissue samples *ex-vivo*. We also demonstrated that such incision can be performed in a fluid with viscosity similar to blood, which is ideal for future use in the field of microrobotics for minimally invasive surgery. The surface friction between the sharp ends and the tissue is believed to facilitate the drilling operation. The advantage of the tubular structure of the microtools is that the hollow structure might be utilized in the future for filling up with drug carrying gels for site directed drill and delivery systems, e.g., cholesterol degrading enzymes for clearing the arterial blockages and plaque removal nanorobots for minimal invasive surgery.

#### ACKNOWLEDGMENT

We thank D. H. Gracias for generating ideas and contribution in the experimental work, C. Deneke for

growing of the MBE samples, S. M. Harazim, A. N. Ananth for help with experiments. S.S. W.X. and O. G. S thank the Volkswagen Foundation (86 362). S. S. thanks the European Research Council (ERC) for Starting Grant “Lab-in-a-tube and Nanorobotics biosensors”.

#### REFERENCES

- [1] a) R. Fernandes and D. H. Gracias, *Mater. Today*, 12 (2009), 14; b) N. Bassik, et al *J. Am. Chem. Soc.*, 132, (2010), 16314; c) A. A. Solovev, et al, *ACS Nano*, 6, (2012), 1751.
- [2] T. E. Mallouk, A. Sen, *Sci. Am.* 300 (2009), 72. b) S. Sanchez, et al, *J. Am. Chem. Soc.*, 133, (2011), 14860. c) S. Sanchez, A. A. Solovev, Y. Mei and O. G. Schmidt, *J. Am. Chem. Soc.*, 132, (2010), 13144. d) M. Pumera. *Chem Commun.*, 47, (2011), 5637. e) S. Sanchez, A. A. Solovev, S. Schulze and O. G. Schmidt, *Chem. Commun.*, 47, (2011), 698. f) S. Sanchez, et al., *J. Am. Chem. Soc.*, 133, (2011), 701.
- [3] B. J. Nelson, I. K. Kaliakatsos and J. J. Abbott, *Annu. Rev. Biomed. Eng.*, 12, (2010), 55. b) K. E. Peyer, L. Zhang and B. J. Nelson *Nanoscale*, 5, (2013) 1259
- [4] S. M. Harazim, W. Xi, C. K. Schmidt, S. Sanchez and O. G. Schmidt, *J. Mater. Chem.* 22, (2012), 2878.
- [5] O.G. Schmidt and K. Eberl, *Nature*, 168, (2001), 410.
- [6] Y. F. Mei, A. A. Solovev, S. Sanchez, O. G. Schmidt. *Chem. Soc. Rev.*, 40, (2011), 2109.
- [7] a) S. Sanchez, et al. *Chem. Rec.* 11, (2011) 367.
- [8] W. Xi, A. A. Solovev, A. N. Ananth, D. H. Gracias, S. Sanchez and O. G. Schmidt. *Nanoscale*, 5, (2013) 1294.

# Approaches to origami-inspired self-folding of printable robots\*

Michael T. Tolley<sup>1</sup>, Samuel M. Felton<sup>1</sup>, Shuhei Miyashita<sup>2</sup>,  
Lily Xu<sup>1</sup>, ByungHyun Shin<sup>1</sup>, Daniela Rus<sup>2</sup>, Robert J. Wood<sup>1</sup>

## I. INTRODUCTION

Engineered systems are typically manufactured using complex 3-D fabrication and assembly processes that are expensive and time consuming. Additionally, complicated infrastructures are usually required for the assembly of these systems. Nature, by contrast, has found an efficient approach to the fabrication of lightweight structures that require little or no infrastructure for deployment: self-folding.

Self-folding structures can be found in biology at length scales from nanometers to meters, such as organic molecules [1], winged insects [2], brains [3], and tree leaves [4], [5]. Self-folding automates the construction of arbitrarily complex geometries at arbitrarily large or small scales. Folding also has many advantages over traditional manufacturing methods, including reduced material consumption and creation of structures with improved strength-to-weight ratios. Folded designs have found useful engineering application in space exploration [6], logistics [7], and robotics [8], [9], [10]. Complimentary theoretical work has proven folding to be capable of achieving a large set of target geometries [11], [12], [13].

Research in small-scale fabrication has developed a variety of self-folding mechanisms. One approach folded lithographically patterned thin films spontaneously via residual stress [14], while another folded hydrogel composites with differential swelling when exposed to water [15]. Layered composites have been shown to self-fold when exposed to a change in pH, temperature, or the addition of a solvent [16]. Self-folding mesoscale structures have been activated by lasers and magnetic fields [17], [18], and complex machines have been assembled via Pop-Up MEMS [19], [20]. In focusing on how to fold structures too small to be directly manipulated in an accurate way, these previous approaches have employed expensive tools and materials, and in many cases used complex infrastructure for deployment (such lasers and magnetic fields).

At the centimeter scale, we have previously used shape memory alloys to actuate a self-folding sheet of pro-

\*The authors gratefully acknowledge support from the National Science Foundation (award numbers CCF-1138967 and EFRI-1240383). Any opinions, findings and conclusions or recommendations expressed in this material are those of the authors and do not necessarily reflect those of the National Science Foundation.

<sup>1</sup>M. T. Tolley, S. M. Felton, L. Xu, B.H. Shin, M. Zhou and R. J. Wood are with the School of Engineering and Applied Sciences and the Wyss Institute for Biologically Inspired Engineering, Harvard University, Cambridge, MA 02138 mtolley@seas.harvard.edu

<sup>2</sup>S. Miyashita and D. Rus are with the Computer Science and Artificial Intelligence Laboratory, Massachusetts Institute of Technology, Cambridge, MA 02139, USA

grammable matter [21]. In designing a universal sheet capable of folding into any shape, this approach relied on the use of complex materials and fabrication approaches, and would not be efficient in the assembly of specific target structures. Recent work has employed selective light absorption to cause inexpensive, single-use shape memory polymers (SMPs) to self-fold into target structures[22]. While this is a simple and inexpensive approach to self-folding, the single-material approach limits the strength and potential applications of the structures formed. Recently, we have demonstrated the use of similar SMPs, selectively actuated by resistive heaters, to realize the self-folding of a single-degree-of-freedom robot [10].

Here we compare three approaches to the fabrication and actuation of low-cost self-folding shape memory laminates. Each approach uses inexpensive, single-use, heat activated SMPs for self-folding, however each uses a unique method of actuating the SMP. The first approach targets the heating of the SMP with selective light absorption, the second localizes SMP actuation using resistive heating elements, and the third achieves folding in uniform environmental heating with an alternative mechanical design. For each approach we describe the design, fabrication, and self-folding of a fundamental structural building block (a cube), as well as a structure to which the approach is uniquely suited to assemble. We then compare and contrast the advantages and disadvantages of each approach.

## II. LIGHT ACTIVATED FOLDING

The basic principle employed in all of our self-folding laminates is akin to a bimorph actuator. In the simplest configuration, a contractile layer is bonded to a mechanical layer. When the contractile layer is activated (induced to contract), the resulting stress cause the bimorph to bend. In order to localize this bending along a fold line, we weaken the mechanical layer at the desired fold location and localize the contraction of the contractile layer above the fold. For light activated heating, black lines are used to preferentially absorb light energy from an infrared light source, localizing the heating of the material underneath. Without this localization, the contractile layer activates indiscriminately and tends to delaminate from the mechanical layer.

For our light activated folding experiments, we used 0.5 mm thick paperboard as a mechanical layer (Fig. 1a) and 0.5 mm thick pre-strained polystyrene sheets (Shrinky Dink, Milton Bradley) as our SMP layer (Fig. 1b). Our chosen SMP was commercially available, inexpensive, and had an activation temperature of approximately 150°C, which is

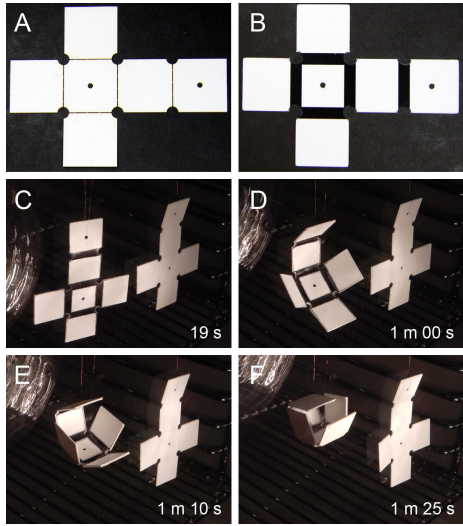


Fig. 1. Light activated self folding of a 20 mm long cube. A) Paperboard and B) SMP layers compose a two-piece laminate. Black lines of ink are printed directly onto the SMP prior to laser machining. C-F) Frames from experiment in which two laminates, one with ink and one without, were introduced into an oven preheated to 90°C. An infrared light was shone through the front glass of the oven. The printed black lines absorb enough light energy to locally activate the SMP.

well above room temperature but below the flash point of paperboard. We printed black ink directly onto the polystyrene sheets with a solid ink printer (ColorQube, Xerox; inkjet printers were also used successfully). We laser machined both materials with a CO<sub>2</sub> laser machining system (VersaLaser, Universal Laser Systems). We aligned the two layers with pins and bonded them with 50  $\mu\text{m}$  double-sided silicone tape (ARclad 7876, Adhesives Research).

As in [22], we found it necessary to pre-heat the SMP to a temperature below the activation temperature. Thus, we suspended the laminates facing the front of an oven preheated to 90°C, and shone an infrared light in through the glass door (Fig. 1d-g). We also suspended an identical laminate without black lines along the hinges in order to verify that it was necessary to localize the light absorption. We observed folding in both cases, although it was much more pronounced and much more regular with ink printed along the hinges (Fig. 1f).

Because light activated folding is inhibited by occlusions, this approach is generally limited to the folding of structures with shallow angles and overall curvatures. This constraint can be relaxed with a movable light source, however this requires additional deployment infrastructure. A strength of this approach, however, is the ability to actuate many folds simultaneously. The Miura fold pattern is thus well suited to this approach. The Miura fold is a regular pattern of folds that result in a single degree-of-freedom when the faces are treated as rigid bodies. It has been proposed as a way to efficiently pack solar panels [6]. With shallow folds it may be a way of improving structure rigidity or function with corrugation.

Following an approach similar to the cube example, we

scored the crease pattern into a sheet of paperboard, and laminated on a sheet of SMP (Fig. 2). Black lines on the SMP defined the valley folds, while the SMP was laser-cut along mountain folds to allow folding. The laminate was heated in an oven with light shone in through the front door. In 2 m 20 s we removed the sample which had formed a Miura fold.

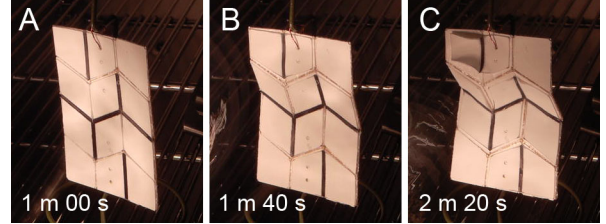


Fig. 2. Light activated Miura fold pattern. Black lines cause the SMP layer to contract, creating valley folds, while cuts in the SMP layer allow mountain folds. A-C) Frames from self-folding experiment with times indicated.

### III. ELECTRICALLY ACTIVATED FOLDING

In order to localize SMP activation without relying on constraining external stimuli such as light, we explored the concept of generating the activating heat within the laminate itself. We achieved this by adding an electrical circuit layer to the laminate which contains resistive heating elements [10]. An additional advantage of this approach is the ability to precisely control a structure's fold sequence. However, this comes at the cost of additional fabrication steps. Here we apply this approach to the self-folding of test structures for comparison with our other self-folding mechanisms.

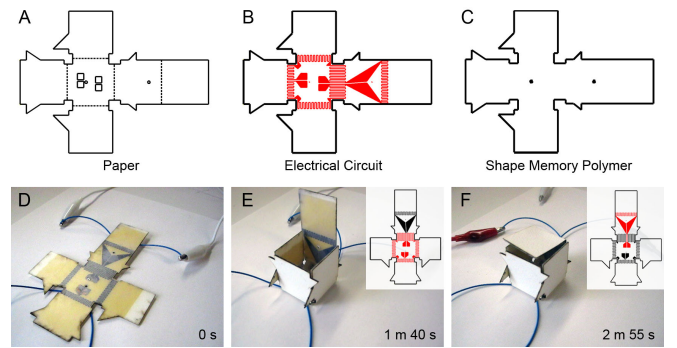


Fig. 3. Electrically activated self-folding cube. A-C) Designs of three layers that compose the electrically activated laminate: a paperboard mechanical layer (A), a copper clad polyimide electrical layer (B), and a pre-strained polystyrene shape memory polymer layer (C). D-F) Frames from self folding experiment. A power supply was used to run two amperes of current through the sub-circuits indicated in red on the insets. The time of each frame is indicated.

We designed a self-folding cube laminate consisting of three layers: a mechanical paperboard layer, an electrical circuit layer, and an SMP layer (Fig. 3a-c). The electrical layer was custom fabricated by first printing a circuit mask with solid ink onto a layer of copper-clad polyimide. The exposed copper was then etched in a heated copper chloride

etch. Finally, the circuit was laser machined, pin-aligned, and bonded to the other layers with silicone tape. The flat laminate can be seen in Fig. 3d. Fig. 3e shows the cube after actuation of the four folds surrounding the bottom face with the resistive heaters highlighted in red in the inset. Due to small differences in actuation rates, some manual intervention was required at this step to prevent these walls from blocking one another. The circuit indicated in Fig. 3f is then used to actuate the remaining fold as shown.

Electrically activated heating is well suited to the folding of structures or devices with minimal infrastructure required (i.e. an electrical power supply). Functional devices are also a good match since there is already an electrical layer embedded in the laminate. Thus, for demonstration purposes we designed and fabricated a self-folding gripper mechanism (Fig. 4). Unactuated folds serve as active degrees of freedom in the folded structure. Strips of polyimide fed through the hollow digits and a slot in the base of the gripper act as artificial tendons which can be pulled on to actuate the device.

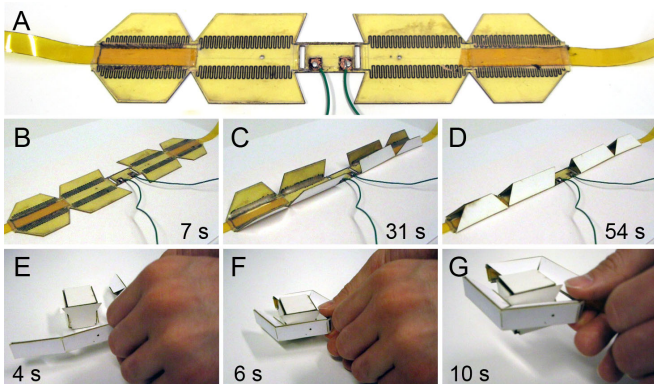


Fig. 4. Self-folding of a functional gripper. A) Self folding laminate with electrical heaters visible as black squarewave shaped lines along self-folding joints. B-D) Frames from self-folding experiment at room temperature. E-G) Frames from experiment demonstrating manual actuation of the gripper by pulling on artificial tendons woven through the digits.

#### IV. UNIFORMLY ACTIVATED FOLDING

The third self-folding approach uses uniform environmental heating as stimulation. In order to prevent heating and contraction of the SMP layer at undesired locations away from the fold lines, a second mechanical layer of paper is added on top of the SMP. A gap of material cut out of this second layer allows the laminate to fold (Fig. 5a). The result is structures that require very little intervention for assembly, or "easy-bake" assembly.

One challenge with this approach is removing gaps of material on the second mechanical layer leaves islands of material that must be aligned properly during fabrication. We solved this problem by leaving a layer of sacrificial material connecting these islands that was removed manually after layer bonding. The designs of three layers of the uniform heating, self-folding cube are shown in (Fig. 5b). Once these layers were stacked and bonded together with silicone tape, the

sacrificial strips between the paper squares on the inside of each cube face were removed manually, leaving the laminate seen in (Fig. 5c). This laminate was inserted into an oven pre-heated to 170°C, and folded into the target shape as shown in less than a minute.

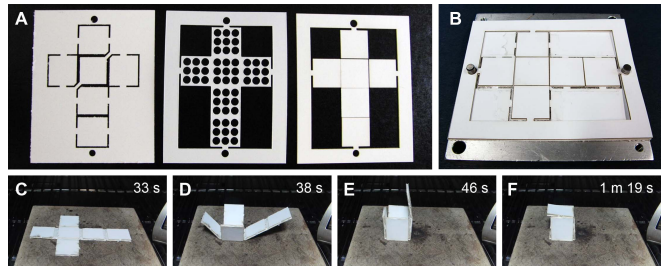


Fig. 5. Fabrication and self-folding of a 20 mm long cube structure with uniform heating. A) Bottom, middle, and top layers of the self-folding composite. The bottom and top layers are 0.5 mm thick paperboard, middle layer is 0.5 mm thick pre-strained polystyrene SMP. B) Pins are used for repeatable laminate alignment, the three layers are stacked and adhered together with silicone tape. C-F) Frames from a self-folding experiment in which the laminate was introduced into an oven preheated to 170°C. Also indicated are the time of each frame from the beginning of the experiment.

Since this uniform heating approach can actuate many folds simultaneously with minimal increase in fabrication complexity, this approach is well suited to the assembly of complex structures that can be assembled with many simultaneous folds. As a demonstration, we fabricated a self-folding icosahedron with 19 actuated folds. Fig. 6 shows the three layers of the laminate, bonding of the three layers with pin alignment, and frames from the self-folding experiment. Based on the results of our angle study, an internal gap width of 1 mm was chosen to achieve a fold angles to match an icosahedron's dihedral angle of 138.2° as closely as possible. Material was also removed from the three-edge intersections to limit the interference of the edges near the vertices of the assembled structure. This structure self-folded in 1 m 04 s into the correct shape but with a gap.

#### V. DISCUSSION

Based on the results of the previous three sections, we can draw some conclusions about the relative advantages and disadvantages of the three approaches to shape memory laminates for automated fabrication. First, light activation was an intriguing method of directing self-folding, but difficult to implement in practice. Unlike a previous implementation of this approach [22], our laminates had to fold the additional weight of the mechanical layer, which we found necessary to add rigidity to the final structures. Due to occlusions, we found it difficult to achieve folds much beyond 90° without manipulation of the target or light source, which limits the usefulness of self-folding. Overall, we found light-activated folding to be most useful for the folding of structures with shallow angles and little structural curvature, such as the Miura pattern presented here.

Electrically activated heating was a consistent approach to self-assembly, although somewhat more complicated in

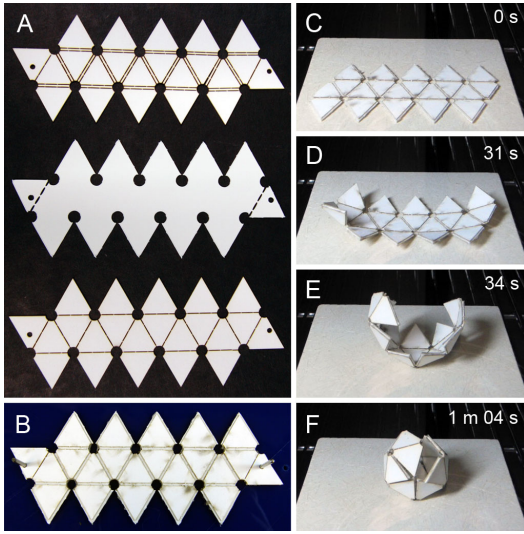


Fig. 6. Fabrication and self-folding of an icosahedron shape. A) Top-bottom: Inner paper layer, SMP layer, outer paper layer. B) Laminate pin alignment, layers are adhered with silicone tape, inner layer bridges are removed after layup. C-F) Frames from self-folding experiment in oven at 170°C with experimental time indicated.

fabrication. This approach had the significant advantage of achieving self-folding at room temperature. It achieved fold angles ranging from 20° to 120°. Because of the capability of sequential actuation, this approach has the potential to achieve the assembly of structures that simultaneous folding methods cannot. The increased control over assembly, as well as the integration of electrical circuitry, mean this approach is well suited to the self-folding of robotic devices such as grippers.

Finally, the uniform heating approach to self-folding shows a great deal of promise as a method that requires very little intervention post-fabrication. This means this approach may scale well both to the fabrication of large batches of structures and to structures with smaller dimensions. The cube fabricated using this method had very little error in side wall alignment. The final alignment of the icosahedron structure was not perfect, but could most likely be improved with design refinement. The main drawbacks of this approach are the requirement of an additional mechanical layer, and the inability to achieve sequential folding. One interesting possibility would be to alleviate this last disadvantage by combining the mechanical alignment of this approach with the electrical heaters of the previous one, gaining the strengths of both.

## VI. CONCLUSIONS

In this paper we have presented three approaches to achieving self-folding with shape memory laminates for automated fabrication: one used light-activation, a second used resistive heaters, and a third used uniform heating with mechanical stops. We fabricated a common structure (a cube) using each approach, demonstrated the strengths of each approach with a unique structure, and compared the advantages and disadvantages of each.

## REFERENCES

- [1] M. S. Z. Kellermayer, S. B. Smith, H. L. Granzier, and C. Bustamante, “Folding-unfolding transitions in single titin molecules characterized with laser tweezers,” *Science*, vol. 276, no. 5315, pp. 1112–1116, 1997.
- [2] F. Haas and R. J. Wootton, “Two basic mechanisms in insect wing folding,” *Proceedings of the Royal Society of London. Series B: Biological Sciences*, vol. 263, no. 1377, pp. 1651–1658, 1996.
- [3] P. Todd, “A geometric model for the cortical folding pattern of simple folded brains,” *Journal of theoretical biology*, vol. 97, no. 3, pp. 529–538, 1982.
- [4] T. Eisner, “Leaf folding in a sensitive plant: A defensive thorn-exposure mechanism?,” *Proceedings of the National Academy of Sciences*, vol. 78, no. 1, pp. 402–404, 1981.
- [5] H. Kobayashi, B. Kresling, and J. F. Vincent, “The geometry of unfolding tree leaves,” *Proceedings of the Royal Society of London. Series B: Biological Sciences*, vol. 265, no. 1391, pp. 147–154, 1998.
- [6] K. Miura, “Method of packaging and deployment of large membranes in space,” in *31st Congress of the International Astronautical Federation*, 1980.
- [7] R. Konings and R. Thijss, “Foldable containers: a new perspective on reducing container-repositioning costs,” *European Journal of Transport and Infrastructure Research*, vol. 1, no. 4, pp. 333–352, 2001.
- [8] C. D. Onal, R. J. Wood, and D. Rus, “Towards printable robotics: Origami-inspired planar fabrication of three-dimensional mechanisms,” in *IEEE Int. Conf. on Robotics and Automation (ICRA)*, pp. 4608–4613, IEEE, 2011.
- [9] C. D. Onal, R. J. Wood, and D. Rus, “An origami-inspired approach to worm robots,” *IEEE/ASME Transactions on Mechatronics*, vol. 18, no. 2, pp. 430–438, 2012.
- [10] S. Felton, M. Tolley, C. D. Onal, D. Rus, and R. J. Wood, “Towards autonomous self-folding: a printed inchworm robot,” in *IEEE Int. Conf. on Robotics and Automation (ICRA)*, p. to be published, IEEE, 2013.
- [11] N. Benbernou, E. D. Demaine, M. L. Demaine, and A. Ovadya, “A universal crease pattern for folding orthogonal shapes,” *Arxiv preprint arXiv:0909.5388*, 2009.
- [12] E. D. Demaine, M. L. Demaine, and J. S. B. Mitchell, “Folding flat silhouettes and wrapping polyhedral packages: New results in computational origami,” *Computational Geometry*, vol. 16, no. 1, pp. 3–21, 2000.
- [13] E. D. Demaine and M. L. Demaine, “Recent results in computational origami,” in *Proceedings of the 3rd International Meeting of Origami Science, Math, and Education*, pp. 3–16, Citeseer, 2001.
- [14] N. Bassik, G. M. Stern, and D. H. Gracias, “Microassembly based on hands free origami with bidirectional curvature,” *Applied physics letters*, vol. 95, no. 9, pp. 091901–091901, 2009.
- [15] J. Guan, H. He, D. J. Hansford, and L. J. Lee, “Self-folding of three-dimensional hydrogel microstructures,” *The Journal of Physical Chemistry B*, vol. 109, no. 49, pp. 23134–23137, 2005.
- [16] L. Ionov, “Soft microorigami: self-folding polymer films,” *Soft Matter*, 2011.
- [17] J. W. Judy and R. S. Muller, “Magnetically actuated, addressable microstructures,” *Journal of Microelectromechanical Systems*, vol. 6, no. 3, pp. 249–256, 1997.
- [18] Y. W. Yi and C. Liu, “Magnetic actuation of hinged microstructures,” *Journal of Microelectromechanical Systems*, vol. 8, no. 1, pp. 10–17, 1999.
- [19] P. Sreetharan, J. Whitney, M. Strauss, and R. Wood, “Monolithic fabrication of millimeter-scale machines,” *Journal of Micromechanics and Microengineering*, vol. 22, no. 5, p. 055027, 2012.
- [20] J. Whitney, P. Sreetharan, K. Ma, and R. Wood, “Pop-up book mems,” *Journal of Micromechanics and Microengineering*, vol. 21, no. 11, p. 115021, 2011.
- [21] E. Hawkes, B. An, N. M. Benbernou, H. Tanaka, S. Kim, E. D. Demaine, D. Rus, and R. J. Wood, “Programmable matter by folding,” *Proceedings of the National Academy of Sciences*, 2010.
- [22] Y. Liu, J. K. Boyles, J. Genzer, and M. D. Dickey, “Self-folding of polymer sheets using local light absorption,” *Soft Matter*, vol. 8, no. 6, pp. 1764–1769, 2012.